

2(mix)

NTIS \$650

EES SERIES REPORT NO. 39

A PROBLEM OF COLLISION AVOIDANCE

Thomas L. Vincent
Eugene M. Cliff
Walter J. Grantham
Willy Y. Peng



Prepared Under NASA Grant No. NGR 03-002-224



(NASA-CR-129988) A PROBLEM OF COLLISION
AVOIDANCE T.L. Vincent, et al (Arizona
Univ., Tucson.) Nov. 1972 86 p

N73-14701

Unclas
G3/21 51855

Reproduced by
NATIONAL TECHNICAL
INFORMATION SERVICE
U S Department of Commerce
Springfield VA 22151

ENGINEERING EXPERIMENT STATION
COLLEGE OF ENGINEERING
THE UNIVERSITY OF ARIZONA
TUCSON, ARIZONA

EES SERIES REPORT NO. 39

A PROBLEM OF COLLISION AVOIDANCE

by

*Thomas L. Vincent
Eugene M. Cliff*
Walter J. Grantham
Willy Y. Peng*

Prepared Under NASA Grant No. NGR 03-002-224

Engineering Experiment Station
College of Engineering
The University of Arizona
Tucson, Arizona

November, 1972

39-11-72-400

*Currently at Virginia Polytechnic Institute and State University,
Blacksburg, Virginia.

PRECEDING PAGE BLANK NOT FILMED

A PROBLEM OF COLLISION AVOIDANCE

by

Thomas L. Vincent
Eugene M. Cliff
Walter J. Grantham
Willy Y. Peng

ABSTRACT

Collision avoidance between two vehicles of constant speed with limited turning radii, moving in a horizontal plane is investigated. Collision avoidance is viewed as a game (in this case, the "game of two cars" defined by Isaacs) by assuming that the operator of one vehicle has perfect knowledge of the state of the other, whereas the operator of the second vehicle is unaware of any impending danger. This situation is perhaps not uncommon in encounters between a light private aircraft and a commercial one and is taken as typical for the results presented.

The situation envisioned is that of an encounter between a commercial aircraft, such as a Boeing 727, and a small light aircraft, such a a Piper Commanche. It is assumed that the pilot of the commercial aircraft has complete information on the state of the light aircraft, but the pilot of the light aircraft is not aware of the presence of the other. His lack of information makes the situation hazardous. He may actually perform a maneuver to cause a collision which might not otherwise occur. This worse case situation is examined to determine the conditions under which the commercial aircraft should execute a collision avoidance maneuver.

Preceding page blank

The answer to this question leads to defining state space zones of vulnerability. Three different zones of vulnerability are defined and the boundaries, or barriers, between these zones are determined for a typical aircraft encounter. A discussion of the methods used to obtain the results as well as some of the salient features associated with the resultant barriers is included.

INTRODUCTION

The high aircraft density of both commercial and private aircraft around large population centers precipitates the likelihood of mid-air collisions. To avoid collisions, air traffic controllers currently attempt to keep track of each aircraft and provide ample warning in cases where collisions "appear" imminent. Their task of keeping track of each aircraft in an air traffic control zone can be alleviated somewhat with the introduction of computers which visually display to the controller the type, velocity, and direction of each aircraft under his command. However, due to uncertainties in aircraft altitude and heading, inaccurate information may be given to the pilots involved. In addition there is a possibility of the controller simply not observing a dangerous situation due to the large number of aircraft involved.

An alternate approach to collision avoidance would be for a pilot to have a "display" at his disposal. Instead of relying on the ground controller to relay information of questionable accuracy, it would be desirable for a pilot to have his own display depicting his vulnerability with respect to other aircraft in his immediate vicinity. This approach falls within the analytical "see and be seen" concept proposed by Stodala (Ref. 1, p. 11), and will be the approach used in this paper. The primary goal will be to determine conditions under which collision avoidance maneuvers would be deemed necessary for an encounter between two aircraft. With this aim in mind, we seek a mathematical model that will lead to a reasonably simple solution and yet, one which will retain the salient features of the problem.

A precise problem statement requires the specification of what knowledge, if any, each pilot has about the dynamical state of the system. Consider the situation in which one of the pilots is "blind" and knows nothing of the dynamical state of the other aircraft. Even though he desires to avoid a collision, his lack of information makes the situation hazardous. He may choose precisely the wrong maneuver and cause a collision. This clearly is a worst-case situation and is the one we will consider in this report.

Specifically, we shall replace the "blind" pilot, who wants to avoid a collision, by a pursuer who wants to cause a collision, and we will treat the problem as a differential game of kind (Ref. 2, p. 8) with two players. One player, the pursuer, attempts to cause a collision while the other player, the evader, attempts to avoid collision.

There are two basic questions involved. First, under what conditions should the evader execute a collision avoidance maneuver? Second, what control action should he take to carry out such a maneuver. These two questions are coupled and are related to three different flight conditions:

1. *Condition Green - the state of the two aircraft is such that if the evader continues in his current direction with constant speed, collision is not possible.*
2. *Condition Yellow - the state of the two aircraft is such that if the evader executes a collision avoidance maneuver, he can escape collision. But if he persists in his current heading and speed, collision is possible.*
3. *Condition Red - the state of the two aircraft is such that, despite any maneuver by the evader, collision is possible.*

The sets of points under conditions green, yellow, and red will be designated by green zone, yellow zone, and red zone respectively.

This report will be primarily concerned with determining the surfaces, or barriers (Ref. 2) in state space which separate these zones. For simplicity, the barrier between the red and yellow zones will be termed the *red barrier*, while the barrier between the yellow and green zones will be termed the *green barrier*.

THE SYSTEM MODEL

The general rigid body motion of a single aircraft could involve a state space consisting of three positional, three velocity, three angular, and three angular velocity coordinates. Thus, the state space for a two aircraft intercept problem could be twenty-four dimensional. In view of the proposed method of solution (investigation of a class of system trajectories) the mere presentation of results would be unmanageable.

Instead, we shall use an aircraft model of point-mass motion in a horizontal plane at a constant speed. This model is relatively simple, and can be reduced to a three-dimensional state space. The constant speed assumption is a reasonable approximation for the time scale of the maneuvers involved. As a typical case, we will consider the collision avoidance problem to be one where the evader is a commercial aircraft such as a Boeing 727 and the pursuer is a small light aircraft such as a Piper Comanche.

In modeling the system, it is assumed that each aircraft moves in a horizontal plane at constant speed, but may turn with a bounded turning rate. This last constraint may result from structural limitations, from power limitations, or from the requirement that the aircraft fly in a horizontal plane in which case the turning rate, $\dot{\beta}$, is related to the bank angle, Φ , and speed, v , of the aircraft by

$$\dot{\beta} = (g \tan \Phi)/v . \quad (1)$$

Here g is the acceleration of gravity and the prime denotes differentiation with respect to time. The lift, L , for horizontal flight is related to the weight, w , by

$$w = L \cos \Phi , \quad (2)$$

and the maximum lift is given by

$$L_{\max} = 1/2 \rho v^2 S (C_L)_{\max} , \quad (3)$$

where ρ is the atmospheric density, S is the wing planform area, and $(C_L)_{\max}$ is the maximum lift coefficient.

From equations (2) and (3)

$$|\Phi|_{\max} = \cos^{-1} \left[2w/\rho v^2 S (C_L)_{\max} \right] , \quad (4)$$

therefore

$$|\dot{\beta}|_{\max} = (g \tan |\Phi|_{\max})/v . \quad (5)$$

Consider now the pursuer, P, and evader, E located in the horizontal plane as shown in Figure 1. The pursuer is moving with constant speed S_P while turning at a rate u . The evader is moving with a constant speed S_E while turning at a rate v . The instantaneous velocity vectors are as indicated with u , v , and x_3 shown positive.

In terms of an evader-centered coordinate system with the x_2 axis aligned with the evader's velocity vector as shown, the kinematical motion of the pursuer relative to the evader is given by

$$\dot{x}_1 = S_P \sin x_3 + vx_2 \quad (6)$$

$$\dot{x}_2 = S_P \cos x_3 - S_E - vx_1 \quad (7)$$

$$\dot{x}_3 = v - u \quad (8)$$

The limitations on the turning rates of the pursuer and evader may be expressed by

$$|u| \leq u_m, \quad |v| \leq v_m. \quad (9)$$

We will now assume that the evader is the faster aircraft and set

$$S_E = 1, \quad S_P = \alpha < 1. \quad (10)$$

We further assume that the maximum turning rate of the evader is less than the pursuer and set

$$v_m = 1, \quad u_m = \delta > 1. \quad (11)$$

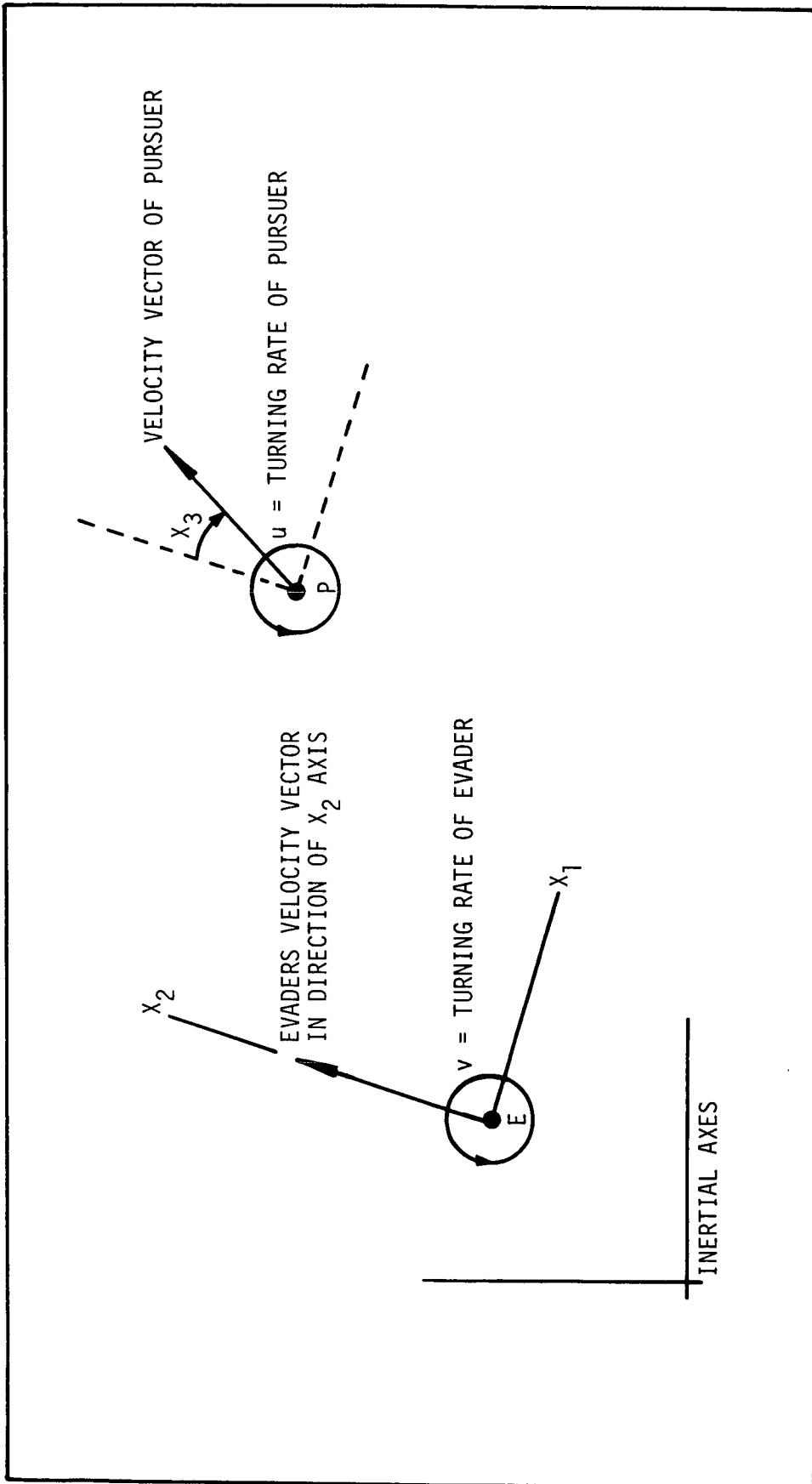


FIGURE 1 PURSUER AND EVADER MOVING IN THE HORIZONTAL PLANE

The kinematical equations, in nondimensional form, become

$$\dot{x}_1 = \alpha \sin x_3 + vx_2 \quad (12)$$

$$\dot{x}_2 = \alpha \cos x_3 - 1 - vx_1 \quad (13)$$

$$\dot{x}_3 = v - u \quad (14)$$

$$|u| \leq \delta, \quad |v| \leq 1 \quad (15)$$

where the dot denotes differentiation with respect to nondimensional time t . The coordinates x_1 and x_2 must be multiplied by S_E/v_m to obtain length dimensions and t must be multiplied by $1/v_m$ to obtain time. Note that $u = +\delta$, $u = 0$, $u = -\delta$ is a hard left turn, straight line flight, and a hard right turn for the pursuer. Similarly $v = +1$, $v = 0$, $v = -1$ is a hard left turn, straight line flight and a hard right turn for the evader.

It will be assumed that collision occurs if the pursuer moves to within a nondimensional radial distance R of the evader. Collision will include the case of tangential encounter at a radius R (see Figure 2). In state space the collision surface is defined to be a cylinder of radius R whose axis is aligned with the x_3 axis.

THE RED BARRIER - A GAME OF KIND (QUALITATIVE GAME)

Points within the red barrier represent states from which the pursuer can guarantee collision with the evader. These points are the analog in game theory to controllable points in control theory and are

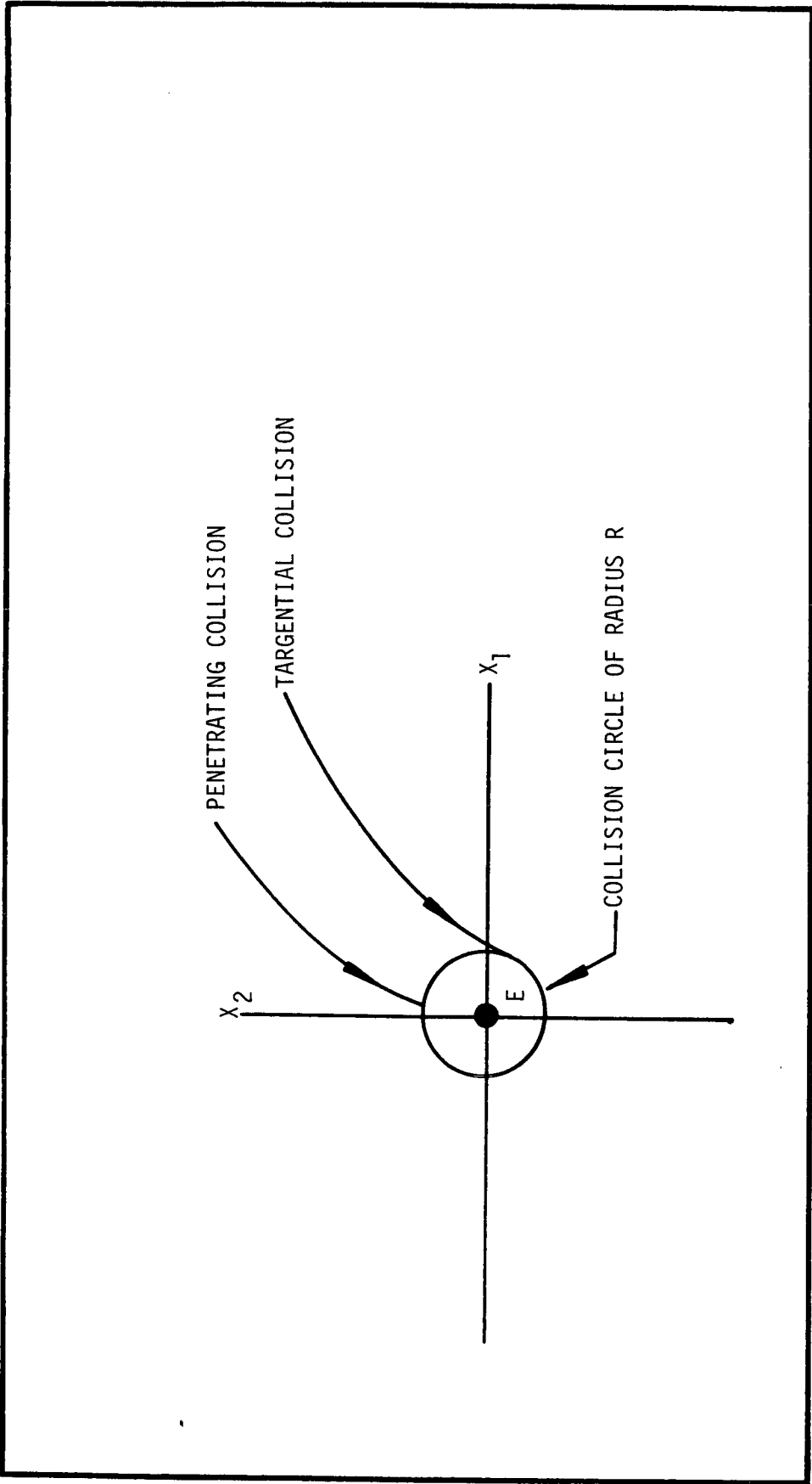


FIGURE 2 EVADER'S VIEW OF COLLISION

determined in a similar way. For systems described by first order differential equations, without state constraints, the boundary of the controllable set may be composed of system trajectories which are obtained from a minimum principle (Ref. 3; Ref. 4, p. 254; Ref. 5, p. 350). (These boundary trajectories may also be thought of as abnormal trajectories for an optimal control problem subject to the same dynamics.) While the boundary delineates those points which are controllable to a terminal set, the determination of the actual feedback control laws used to drive the system to the terminal set from within the boundaries represents a separate (more difficult) problem.

The red zone is similar. Solving a game of kind involves the determination of a "game surface" with particular properties. If two game surfaces emanating from the collision surface intersect, then the resulting enclosed points may represent guaranteed collision points. Again, while it may be known that collision is guaranteed in the red zone, a solution to the game of kind (determination of game surfaces) does not yield a priori collision maneuvers for points within the red zone.

The game of kind was defined by Isaacs (Ref. 2, p. 200-231) and has been extensively investigated by Blaquiere, et al (Ref. 6, p. 103-145). The methods of these authors will be used here. Points in the red zone are those points which are enclosed by intersecting game surfaces and the collision surface. A game surface and the intersection of these surfaces is depicted in Figure 3. If u and v represent controls which will maintain a system on a game surface, then this surface is

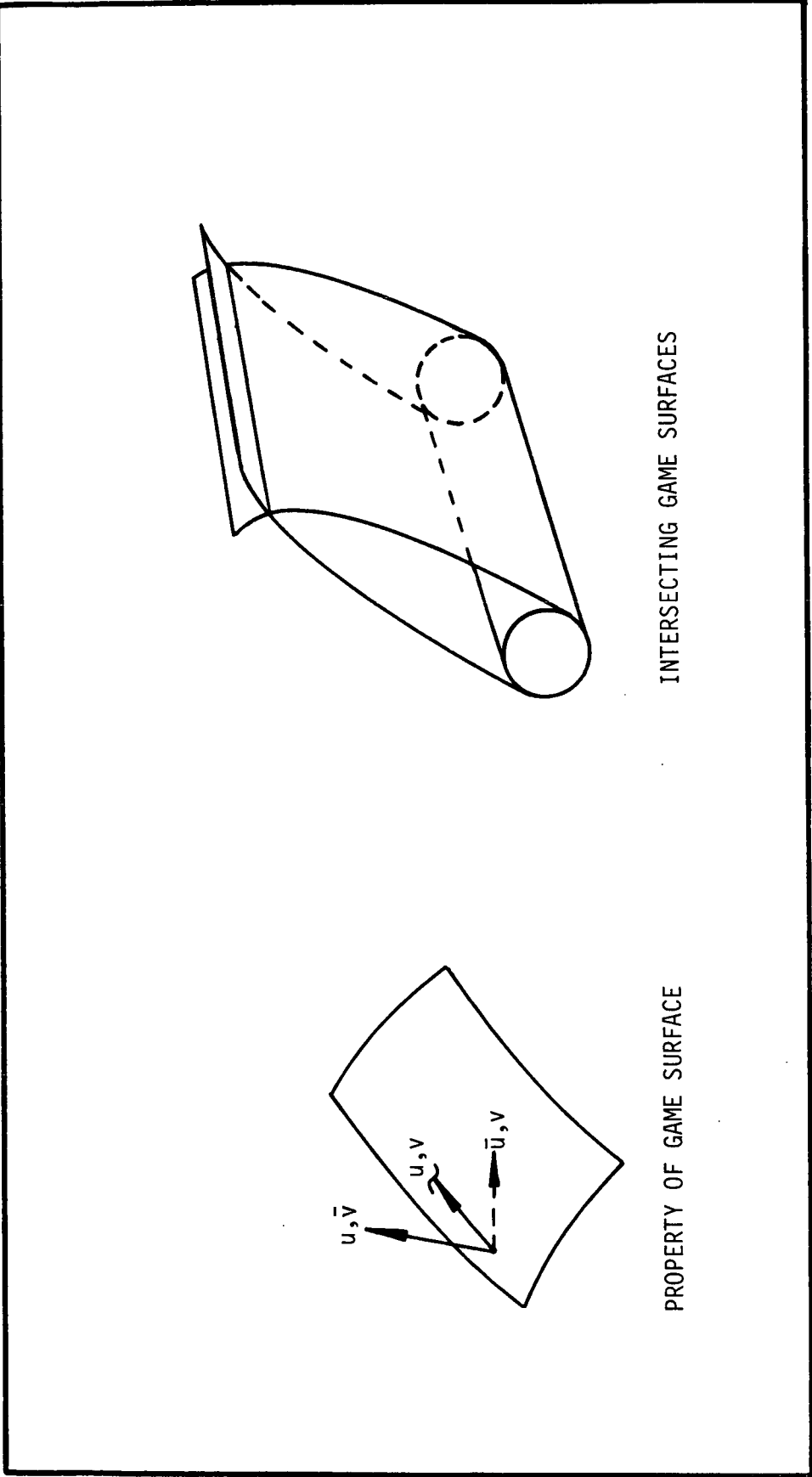


FIGURE 3 DETERMINATION OF THE RED BARRIER

defined to have the property that a control pair (u, \bar{v}) will move the system along or to one side of the surface whereas the control pair (\bar{u}, v) will move the system along or to the other side of the surface. In effect, a game surface divides the space, at least locally, into regions in which one or the other player can force the system to remain. If two such surfaces emanating from the collision surface intersect, and if the enclosed points correspond to (u, \bar{v}) control (see Figure 3) then such points are guaranteed collision points for the pursuer. Game theory not only dictates the game surface control, but the proper points on a terminal set (collision surface) for constructing the boundaries of the red zone.

Red Barrier Necessary Conditions

From Theorem 6.1, p. 131 of reference 6, if u and v are game surface controls for $t \in [0, t_f]$ for the dynamical system

$$\dot{x} = f(x, u, v) \quad (16)$$

where

$$x^T = [x_1 \dots x_n] \in \underline{GCE}^n, \quad u^T = [u_1 \dots u_r] \in \underline{UCE}^r, \quad v^T = [v_1 \dots v_s] \in \underline{VCE}^s,$$

and where the function f is of class C^1 on $GxUxV$ and if we let

$$H = \lambda^T f(x, u, v) \quad (17)$$

where $\lambda^T = [\lambda_1 \dots \lambda_n] \in E^N$, then there exists a nonzero continuous solution of the adjoint equation

$$\dot{\lambda}^T = - \partial H / \partial x \quad (18)$$

such that for any controls \bar{u}, \bar{v} other than u, v

$$H(\lambda, x, u, \bar{v}) \leq H(\lambda, x, u, v) \leq H(\lambda, x, \bar{u}, v) \quad (19)$$

$$H(\lambda, x, u, v) = 0 \quad (20)$$

for all $t \in [0, t_f]$. Furthermore, for the problem under consideration (boundary of red zone for cylindrical collision surface) the vector λ at the terminal surface is in the direction of the outward normal to the surface.

From (12), (13), and (14) we thus have

$$H = \lambda_1 (\alpha \sin x_3 + v x_2) + \lambda_2 (\alpha \cos x_3 - 1 - v x_1) + \lambda_3 (v - u) \quad (21)$$

with the adjoint system

$$\dot{\lambda}_1 = \lambda_2 v \quad (22)$$

$$\dot{\lambda}_2 = - \lambda_1 v \quad (23)$$

$$\dot{\lambda}_3 = \alpha (\lambda_2 \sin x_3 - \lambda_1 \cos x_3) \quad (24)$$

Red Barrier Control

The function H is linear in the controls u and v and for convenience is written as

$$H = \lambda_1 \alpha \sin x_3 + \lambda_2 (\alpha \cos x_3 - 1) + \sigma_u u + \sigma_v v \quad (25)$$

where $\sigma_u = -\lambda_3$ and $\sigma_v = \lambda_1 x_2 - \lambda_2 x_1 + \lambda_3$. To satisfy (19) we conclude

$$u = \begin{cases} +\delta & \text{if } \sigma_u < 0 \\ -\delta & \text{if } \sigma_u > 0 \\ \text{singular control} & \text{if } \sigma_u = 0 \end{cases} \quad (26)$$

$$v = \begin{cases} +1 & \text{if } \sigma_v > 0 \\ -1 & \text{if } \sigma_v < 0 \\ \text{singular control} & \text{if } \sigma_v = 0 \end{cases} \quad (27)$$

That is, the signs of the "switching functions" σ_u and σ_v determine the controls to be used, unless the switching function is identically zero. This latter possibility is examined by setting the first and second order time derivatives of σ_u and σ_v equal to zero. We obtain

$$\dot{\sigma}_u = \alpha(\lambda_1 \cos x_3 - \lambda_2 \sin x_3) \quad (28)$$

$$\ddot{\sigma}_u = \alpha u (\lambda_1 \sin x_3 + \lambda_2 \cos x_3) \quad (29)$$

$$\dot{\sigma}_v = -\lambda_1 \quad (30)$$

$$\ddot{\sigma}_v = -\lambda_2 v \quad (31)$$

Thus from $\ddot{\sigma}_u = \ddot{\sigma}_v = 0$ we obtain for pursuer singular control either $u = 0$ or $(\lambda_1 \sin x_3 + \lambda_2 \cos x_3) = 0$ and for evader singular control

either $v = 0$ or $\lambda_2 = 0$. It can be shown using $\dot{\sigma}_u = \dot{\sigma}_v = 0$ that in each case the second choices require that $\lambda^T = 0$ and hence are not possible solutions. We conclude then that singular controls for both the pursuer and the evader corresponds to null control.

We say that collision occurs when the pursuer is within a given radius R of the evader. If we designate quantities evaluated at the terminal or final time with the subscript "f", then the collision surface is written as

$$\theta \equiv x_{1f}^2 + x_{2f}^2 - R^2 = 0 . \quad (32)$$

The gradient to this surface (in x_1, x_2, x_3 space) is directed outward so that the terminal condition for the λ vector may be given by

$$\lambda_f^T = \mu \frac{\partial \theta}{\partial x_f} \quad (33)$$

where μ is a positive constant. We thus have

$$\lambda_{1f} = 2\mu x_{1f} \quad (34)$$

$$\lambda_{2f} = 2\mu x_{2f} \quad (35)$$

$$\lambda_{3f} = 0 . \quad (36)$$

Substituting this information into $H_f = 0$ yields

$$x_{2f}/x_{1f} = \alpha \sin x_{3f} / (1 - \alpha \cos x_{3f}) . \quad (37)$$

Condition (37) requires that a game surface trajectory be tangent to the terminal manifold, i.e., collisions resulting from initial states on the red barrier are "side-swipes" or "non-penetrating" collisions.

We may now examine the control possibilities at termination. From (34-35) we see that both switching functions are zero on the terminal manifold. We examine first the possibility of singular control. Pursuer singular control requires that $\dot{\sigma}_{uf} = 0$. This condition along with (34), (35), and (37) all evaluated on the terminal surface yields

$$\cos x_{3f} = \alpha \quad . \quad (38)$$

Evader singular control requires that $\dot{\sigma}_{vf} = -\lambda_{1f} = 0$. From (36), $\lambda_{3f} = 0$, thus from the requirement that $H_f = 0$ we have either $\lambda_{2f} = 0$ or $\cos x_{3f} = 1/\alpha$. The first condition would require $\lambda_f^T = 0$ and is not possible, the second condition cannot be satisfied with $\alpha < 1$ (as assigned). We conclude that terminal evader singular control is not possible and that terminal pursuer singular control is possible when $\cos x_{3f} = \alpha$.

For non-singular terminal control we observe that

$$u_f = + \delta \text{ requires } \dot{\sigma}_{uf} \geq 0 \quad (39)$$

$$u_f = - \delta \text{ requires } \dot{\sigma}_{uf} \leq 0 \quad (40)$$

$$v_f = + 1 \text{ requires } \dot{\sigma}_{vf} \leq 0 \quad (41)$$

$$v_f = -1 \text{ requires } \dot{\sigma}_{vf} \geq 0 \quad . \quad (42)$$

By substituting (34) and (35) into (28) and (30) we observe that when $x_{1f} > 0$ (for points on the right half of the capture circle)

$$v_f = +1 \quad (43)$$

$$u_f = +\delta \text{ when } \cos x_{3f} \geq \alpha \quad (44)$$

$$u_f = -\delta \text{ when } \cos x_{3f} \leq \alpha \quad (45)$$

and when $x_{1f} < 0$ (for points on the left half of the capture circle)

$$v_f = -1 \quad (46)$$

$$u_f = +\delta \text{ when } \cos x_{3f} \leq \alpha \quad (47)$$

$$u_f = -\delta \text{ when } \cos x_{3f} \geq \alpha \quad . \quad (48)$$

Thus terminal control is uniquely specified except when $\cos x_{3f} = \alpha$. At such a point the pursuer controls $u = \pm \delta$, and $u = 0$ all satisfy the necessary conditions examined so far. The possibility of singular control at such a point will now be examined in further detail.

For convenience in what follows we define x_3^* as the angle between 0 and $\pi/2$ such that $\alpha = \cos x_3^*$. Thus $\dot{\sigma}_u(t_f) = 0$ at $x_3(t_f) = x_3^*$ and at $x_3(t_f) = 2\pi - x_3^*$. A necessary condition for the singular pursuer control $u = 0$ to minimize the Hamiltonian (Ref. 6, p. 69) is

$$\frac{\partial}{\partial u} (\ddot{\alpha}_u) \leq 0 \quad . \quad (49)$$

Applying this condition to (29) evaluated at the terminal point requires

$$x_{1f} \sin x_{3f} + x_{2f} \cos x_{3f} \leq 0 \quad . \quad (50)$$

By use of (37) we see that this requires that

$$\sin x_{3f} \leq 0 \quad (51)$$

on the right side of the collision surface ($x_{1f} > 0$) and

$$\sin x_{3f} \geq 0 \quad (52)$$

on the left side of the collision surface ($x_{1f} < 0$). Thus singular control is possible only at $x_3(t_f) = 2\pi - x_3^*$ with $x_{1f} > 0$ and at $x_3(t_f) = x_3^*$ with $x_{1f} < 0$.

Necessary conditions thus provide for the following terminal control possibilities for $x_{3f} \in [0, 2\pi]$. On the right side ($x_{1f} > 0$):

$$v_f = +1$$

$$u_f = \begin{cases} +\delta \text{ for } x_{3f}: & x_{3f} \in [0, x_3^*] \cup [2\pi - x_3^*, 2\pi] \\ 0 \text{ for } x_{3f}: & x_{3f} = 2\pi - x_3^* \\ -\delta \text{ for } x_{3f}: & x_{3f} \in [x_3^*, 2\pi - x_3^*] \end{cases} \quad (53)$$

On the left side ($x_{1f} < 0$):

$$\begin{aligned}
 v_f &= -1 \\
 u_f &= \begin{cases} -\delta \text{ for } x_{3f}: & x_{3f} \in [0, x_3^*] \cup [2\pi - x_3^*, 2\pi] \\ 0 \text{ for } x_{3f}: & x_{3f} = x_3^* \\ +\delta \text{ for } x_{3f}: & x_{3f} \in [x_3^*, 2\pi - x_3^*] \end{cases} \quad (54)
 \end{aligned}$$

Retrograde Integration

The game surface emanating from the right side of the collision surface ($x_{1f} > 0$) will be called the *right red barrier*, and the game surface emanating from the left side will be called the *left red barrier*.

Trajectories which lie in the game surfaces may be calculated by integrating the equations of motion and the adjoint equations backward from the collision surface using controls obtained from the Minimum Principle (19). Integration is initiated using the controls given by (53) and (54). By obtaining a number of such trajectories the nature of the red zone can be determined.

The red zone is a three dimensional set of points in x_1, x_2, x_3 space whose boundaries are composed of the barriers and the collision surface. The red zone is perhaps best depicted by plotting x_1 vs. x_2 cross sections of it for various values of x_3 . This will be the method used here to depict the results.

For what follows, note that singular control for the evader on a barrier is never optimal, and all references to singular control henceforth refer to terminal u - singular control.

Trajectories which lie on the barriers are of two types. The first type, called Π trajectories, terminate non-singularly, i.e., with $u(t_f) \neq 0$. The second type, called Π^* trajectories, terminate with u - singular control.

To integrate backwards we define the "time-to-go"

$$\tau \triangleq t_f - t . \quad (55)$$

Using τ as the independent variable in the equations of motion and the adjoint equations gives

$$\dot{x}_1(\tau) = -\alpha \sin x_3(\tau) - x_2(\tau)v , \quad (56)$$

$$\dot{x}_2(\tau) = -\alpha \cos x_3(\tau) + x_1(\tau)v + 1 , \quad (57)$$

$$\dot{x}_3(\tau) = u - v , \quad |v| \leq 1 , \quad |u| \leq \delta , \quad (58)$$

$$\dot{\lambda}_1(\tau) = -v\lambda_2(\tau) , \quad (59)$$

$$\dot{\lambda}_2(\tau) = v\lambda_1(\tau) , \quad (60)$$

$$\dot{\lambda}_3(\tau) = \alpha\{\lambda_1(\tau) \cos x_3(\tau) - \lambda_2(\tau) \sin x_3(\tau)\} , \quad (61)$$

where $(\dot{})$ denotes differentiation with respect to τ . The "initial

conditions" for these retro-equations are given by (32) and (34-37) where the final time must now be interpreted as an initial time.

For this particular problem an analytic solution exists for the above equations and is easily constructed through the use of another change of independent variable.

Let $[\tau_0, \tau_s]$ be a (retro) time interval over which σ_u and σ_v do not change sign, i.e. starting with

$$\sigma_u(\tau_0) = \sigma_v(\tau_0) = 0, \quad (62)$$

define

$$\tau_u \triangleq \text{first time } \sigma_u = 0 \text{ after being non-zero} \quad (63)$$

$$\tau_v \triangleq \text{first time } \sigma_v = 0 \text{ after being non-zero} \quad (64)$$

then

$$\tau_s \triangleq \min(\tau_u, \tau_v). \quad (65)$$

The Π trajectories are obtained by integrating the retro-equations using non-singular control on the interval $0 \leq \tau \leq \tau_s$. If τ^* is the (retro) time at which the pursuers control switches from singular to non-singular, then the Π^* trajectories are obtained by first integrating the retro-equations using singular control on the interval $0 \leq \tau \leq \tau^*$ and continuing integration using non-singular control on the interval $\tau^* \leq \tau \leq \tau_s$.

Let $\tau_0 = 0$ for Π trajectories and $\tau_0 = \tau^*$ for Π^* trajectories, then $x_3(\tau)$ is a constant on the interval $\tau_0 \leq \tau \leq \tau^*$ for both Π and Π^* trajectories. Thus the following relation exists between differentiation with respect to τ and differentiation with respect to x_3 :

$$\frac{d(\)}{d\tau} = (u - v) \frac{d(\)}{dx_3} . \quad (66)$$

Using this relation, the retro-equations become

$$x_1' = -\Omega(\alpha \sin x_3 + x_2 v)/v \quad (67)$$

$$x_2' = \Omega(1 - \alpha \cos x_3 + x_1 v)/v , \quad (68)$$

$$\lambda_1' = -\Omega\lambda_2 , \quad (69)$$

$$\lambda_2' = \Omega\lambda_1 , \quad (70)$$

$$\lambda_3' = \alpha\Omega(\lambda_1 \cos x_3 - \lambda_2 \sin x_3)/v \quad (71)$$

where

$$\Omega \triangleq v/(u - v) \quad (72)$$

$$x_3(\tau) = (u - v)(\tau - \tau_0) + x_3(\tau_0) , \quad (73)$$

and ()' denotes differentiation with respect to x_3 .

It should be noted that the change of (independent) variable given by equation (73) is subject to two constraints. First the actual range of x_3 must be such that the corresponding value of τ is $\geq \tau_0$. Second, the change of variable is meaningless if $v = u$. Since $v \neq 0$, this could occur only if $\delta = 1$. However, for a collision avoidance problem in which the pursuer has a larger maximum turning rate ($\delta > 1$), this difficulty does not arise.

The II Trajectories

Integration of equations (67 - 71) yields the non-singular trajectory (subarc) equations

$$\begin{aligned}
 x_1 = & x_1(\tau_0) \cos \Omega[x_3 - x_3(\tau_0)] - x_2(\tau_0) \sin \Omega[x_3 - x_3(\tau_0)] \\
 & + \alpha[\cos x_3 - \cos\{\Omega[x_3 - x_3(\tau_0)] - x_3(\tau_0)\}]/u \quad (74) \\
 & + \{\cos \Omega[x_3 - x_3(\tau_0)] - 1\}/v ,
 \end{aligned}$$

$$\begin{aligned}
 x_2 = & x_1(\tau_0) \sin \Omega[x_3 - x_3(\tau_0)] + x_2(\tau_0) \cos \Omega[x_3 - x_3(\tau_0)] \\
 & - \alpha[\sin x_3 + \sin\{\Omega[x_3 - x_3(\tau_0)] - x_3(\tau_0)\}]/u \quad (75) \\
 & + \sin \Omega[x_3 - x_3(\tau_0)]/v ,
 \end{aligned}$$

and, the switching functions

$$\begin{aligned} \sigma_v &= \{x_1(\tau_0) \sin \Omega[x_3 - x_3(\tau_0)]\}/v \\ &+ x_2(\tau_0) \{\cos \Omega[x_3 - x_3(\tau_0)] - 1\}/v + \sigma_v(\tau_0) \end{aligned} \quad (76)$$

and

$$\begin{aligned} \sigma_u &= -\alpha x_1(\tau_0) [\sin \{\Omega[x_3 - x_3(\tau_0)] + x_3\} - \sin x_3(\tau_0)]/u \\ &- \alpha x_2(\tau_0) [\cos \{\Omega[x_3 - x_3(\tau_0)] + x_3\} \\ &- \cos x_3(\tau_0)]/u + \sigma_u(\tau_0) , \end{aligned} \quad (77)$$

where μ , in equations (34 - 35) has been taken as + 1.

For the totally non-singular Π trajectories, we set $\sigma_u(\tau_0) = \sigma_v(\tau_0) = \tau_0 = 0$ and $x_1(0)$ and $x_2(0)$ are given by equations (32) and (37) for a specified $x_{3f} = x_3(0)$.

The Π^* Trajectories

The Π^* trajectories are initially u-singular and integration of equations (67 - 71) with $u = 0$ and $\tau_0 = 0$ gives the singular arc equations

$$\begin{aligned} x_1 &= x_1(0) \cos [x_3 - x_3(0)] + x_2(0) \sin [x_3 - x_3(0)] \\ &+ \alpha \sin x_3 [x_3 - x_3(0)]/v + \{\cos [x_3 - x_3(0)] - 1\}/v \end{aligned} \quad (78)$$

$$x_2 = -x_1(0) \sin [x_3 - x_3(0)] + x_2(0) \cos [x_3 - x_3(0)] \quad (79)$$

$$+ \alpha \cos x_3 [x_3 - x_3(0)]/v - \{\sin[x_3 - x_3(0)]\}/v$$

$$x_3 = x_3(0) - v\tau, \quad (80)$$

and the switching functions

$$\sigma_v = - [x_1(0) \sin [x_3 - x_3(0)] - x_2(0) \{\cos[x_3 - x_3(0)] - 1\}] / v, \quad (81)$$

$$\sigma_u = 0, \quad (82)$$

where $x_1(0)$ and $x_2(0)$ are given by equations (32) and (37) with $x_{3f} = x_3(0) = x_3^*$ on the left side and $x_{3f} = x_3(0) = 2\pi - x_3^*$ on the right side.

At $\tau = \tau^*$ the pursuer switches from singular to non-singular control, and the remaining non-singular portion of the Π^* trajectory is computed from equations (74 - 77) with $\tau_0 = \tau^*$ and with the "initial conditions" $x_1(\tau_0)$, $x_2(\tau_0)$, $x_3(\tau_0)$, $\sigma_u(\tau_0)$, and $\sigma_v(\tau_0)$ computed from equations (78 - 82) at τ^* .

Some Observations for a Specific Case

The procedure suggested here of integrating the retro-equations until $\tau = \tau_s$ leaves open the question of control sequences for $\tau > \tau_s$. Numerical results (with $\alpha = .5$, $\delta = 2.5$, $R = 0.02$) yield the following observations: The point on a given trajectory corresponding to $\tau = \tau_s$

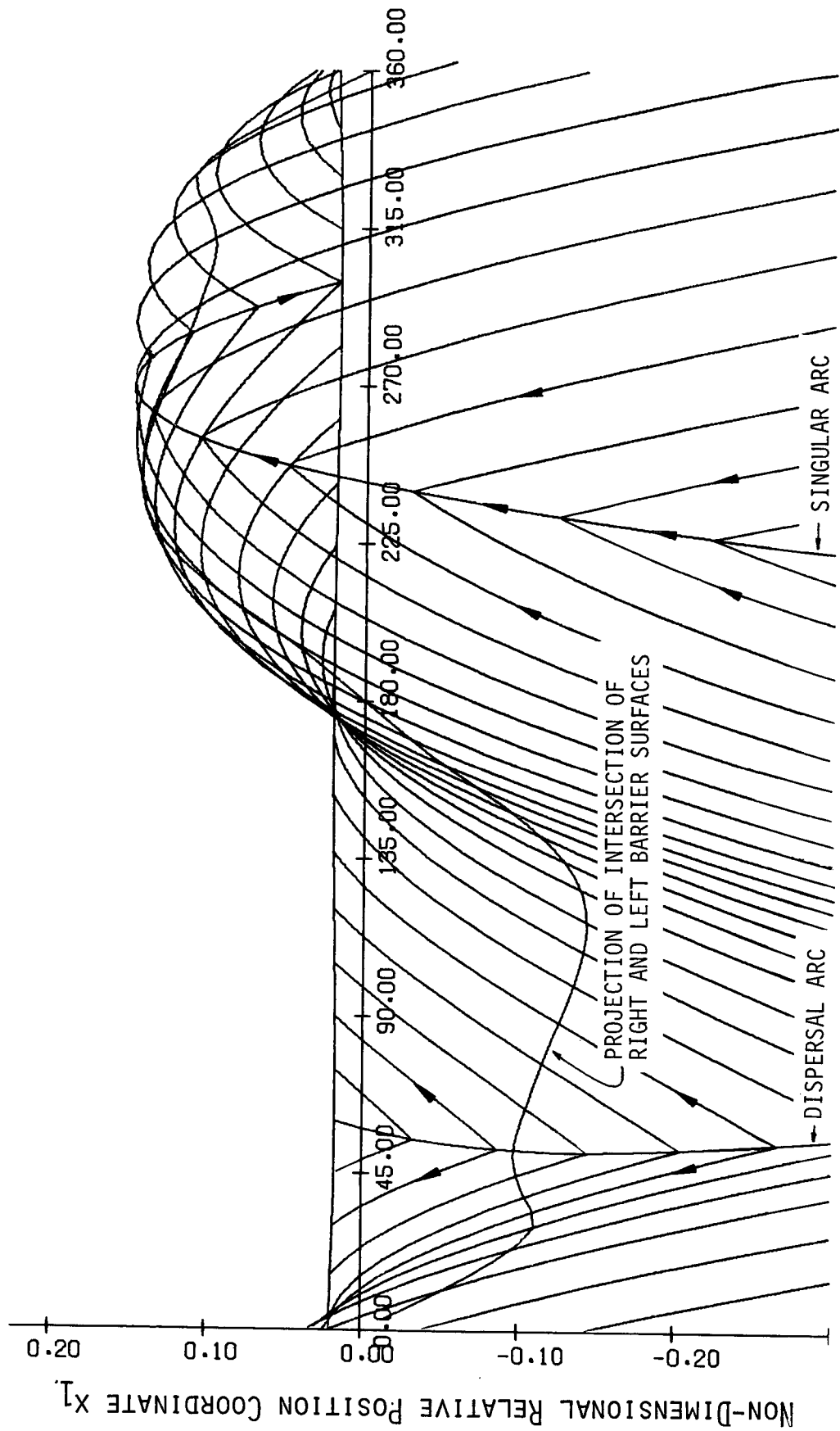
always lies off the barrier. It follows then that a trajectory on the barrier has at most one switch, and if a switch occurs it is from singular to non-singular control (in the retro sense, i.e., Π^* trajectories). Figures 4 - 7 show, for the case of $\alpha = 0.5$, $\delta = 2.5$, and $R = 0.02$, the projection of trajectories onto the $x_1 - x_3$ and $x_2 - x_3$ plane. The direction of motion indicated is that of forward integration.

In the retrograde sense, trajectories in Figures 4 and 5 starting above and below $x_{3f} = 60^\circ$ intersect. The points of intersection generate a dispersal curve whose projection is shown in the figures. It is of interest to note that for a point on the dispersal curve the time to collision (in the forward sense) differs depending on the choice of trajectories.

A second curve of interest shown on these curves is the singular arc which intersects $x_3(t_f)$ at 300° . The Π^* type of trajectories all switch to singular control upon intersecting this arc.

The trajectories of Figures 4 and 5 lie on the left red barrier and the trajectories of Figures 6 and 7 lie on the right red barrier. These barriers are surfaces which intersect in the manner depicted in Figure 3 and points enclosed by the left and right red barrier and the terminal surface are within the red zone. Projections of the points of intersection are also shown in Figure 4 - 7.

While points which lie on the curve defined by the intersection of the right and left barriers are guaranteed collision points for the pursuer, his choice of control at such points (i.e. left barrier control or right barrier control) is not arbitrary for certain situations.



RELATIVE ANGLE x_3

FIGURE 4 TRAJECTORIES ON AN x_1 - x_3 PROJECTION OF THE RIGHT RED BARRIER

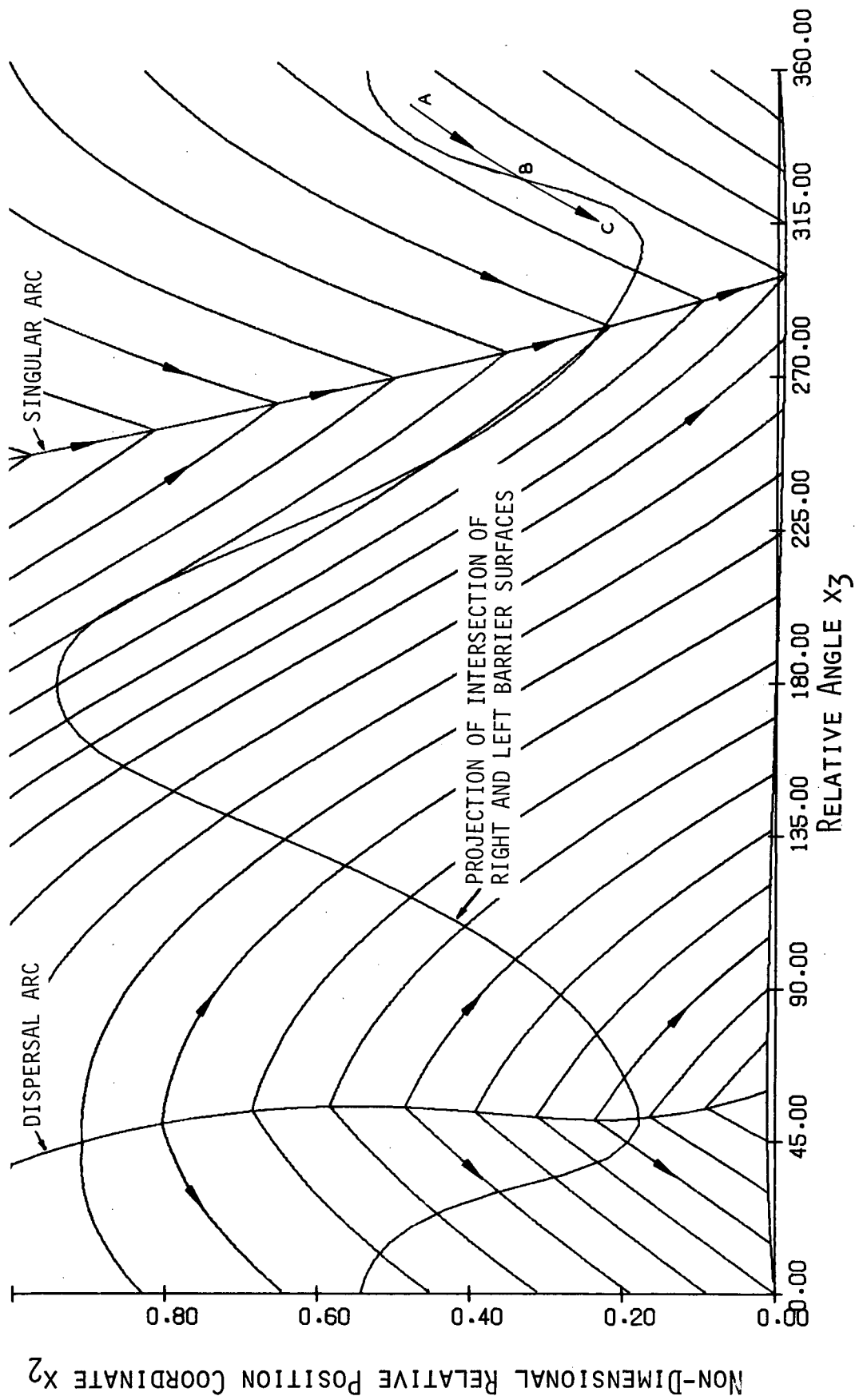


FIGURE 5 TRAJECTORIES ON AN X_2 - X_3 PROJECTION OF THE RIGHT RED BARRIER

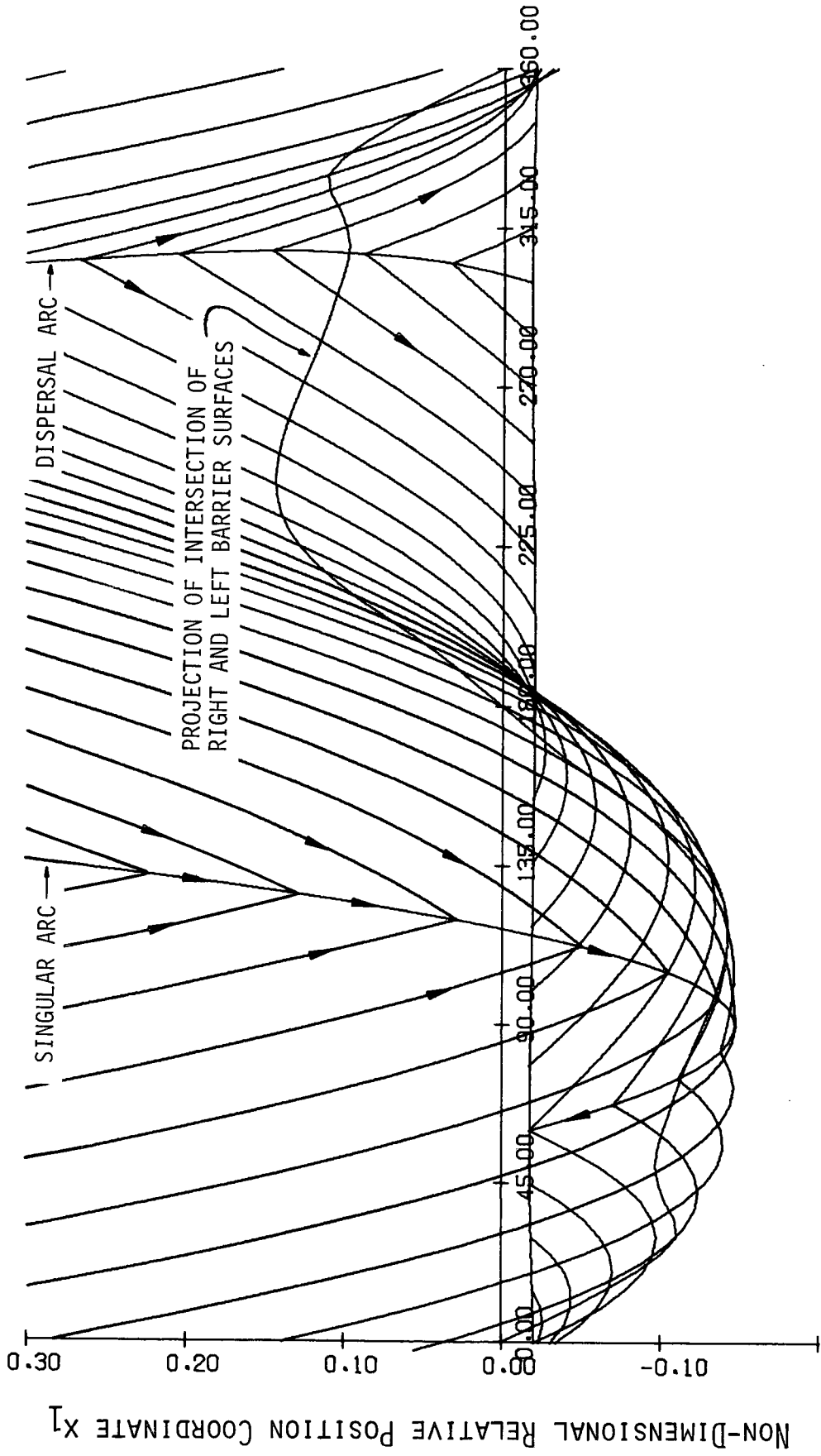


FIGURE 6 TRAJECTORIES ON AN x_1 - x_3 PROJECTION OF THE LEFT RED BARRIER

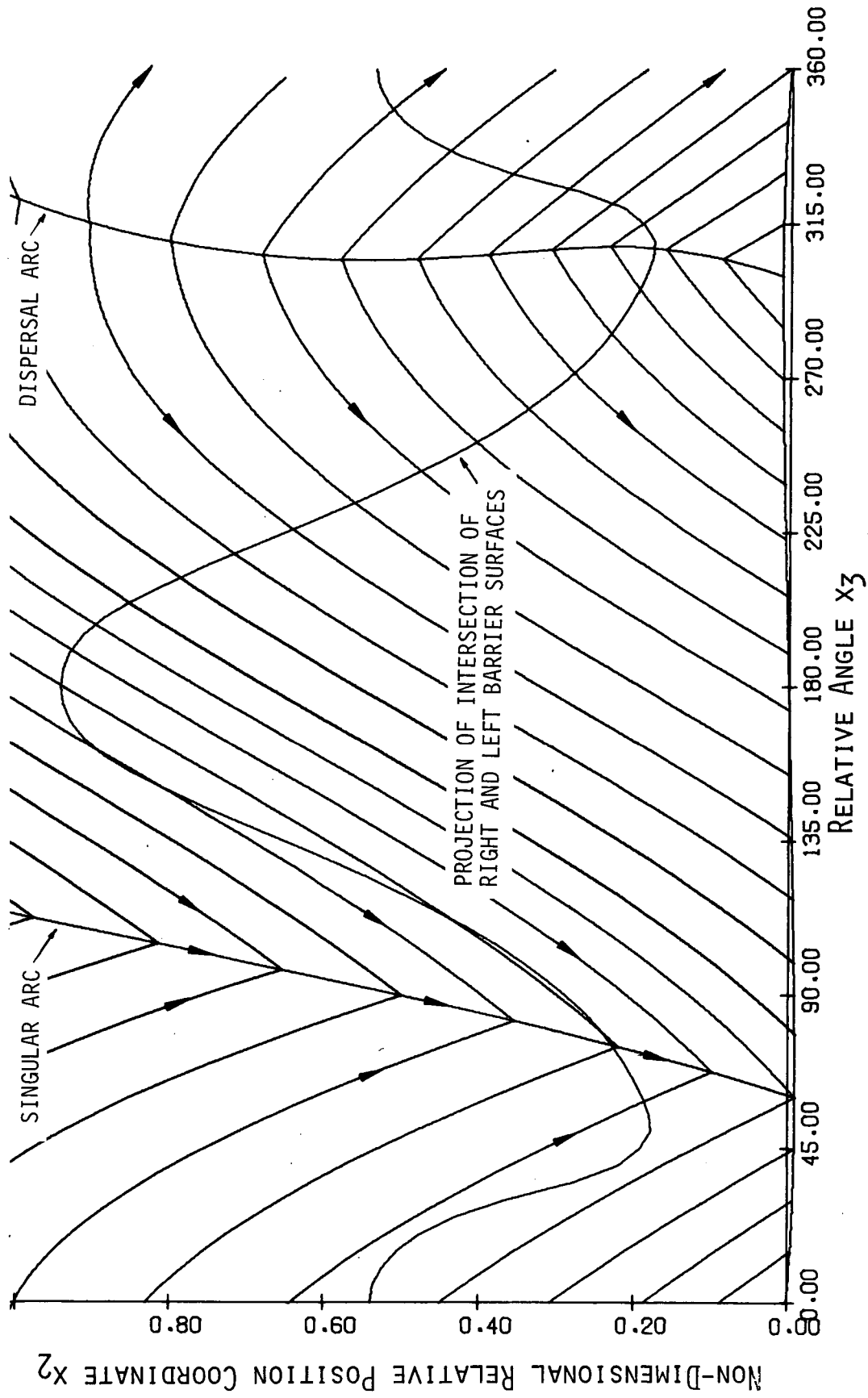


FIGURE 7 TRAJECTORIES ON AN X_2 - X_3 PROJECTION OF THE LEFT RED BARRIER

This condition is best illustrated by examining the motion of a barrier trajectory in the vicinity of the intersection of barriers.

Figure 8 represents a type of motion which is common for a number of trajectories on the barriers. Starting at some points on the left or right barrier in the vicinity of, but not on the curve of barrier intersection, the corresponding game surface trajectory moves the system to an intersection point. For example, the point A (see also Figure 5)* on the right red barrier is such a point. In the forward sense, the game surface trajectory moves from A to B with the pursuer and evader both using right barrier controls. If the pursuer continues with right barrier control, the evader can then move the system to the point C (outside the red zone) by simply continuing with his right barrier control. However if the pursuer switches at B to left barrier control then the system will either move down the left barrier or into the red zone depending upon whether the evader either uses left barrier control or some other admissible control. We conclude then that the point B (a point on the intersection of the left and right barriers) is a guaranteed capture point for the pursuer provided that he uses left barrier control. This same sort of situation where the choice of control at the intersection of barriers is not arbitrary occurs at a number of other intersection points. Indeed this condition will present itself at any point where the barrier intersection slope is the same sign, but of greater magnitude than trajectory slopes.

*Points A, B, and C are projections onto $x_2 - x_3$ of points that lie on the same trajectory.

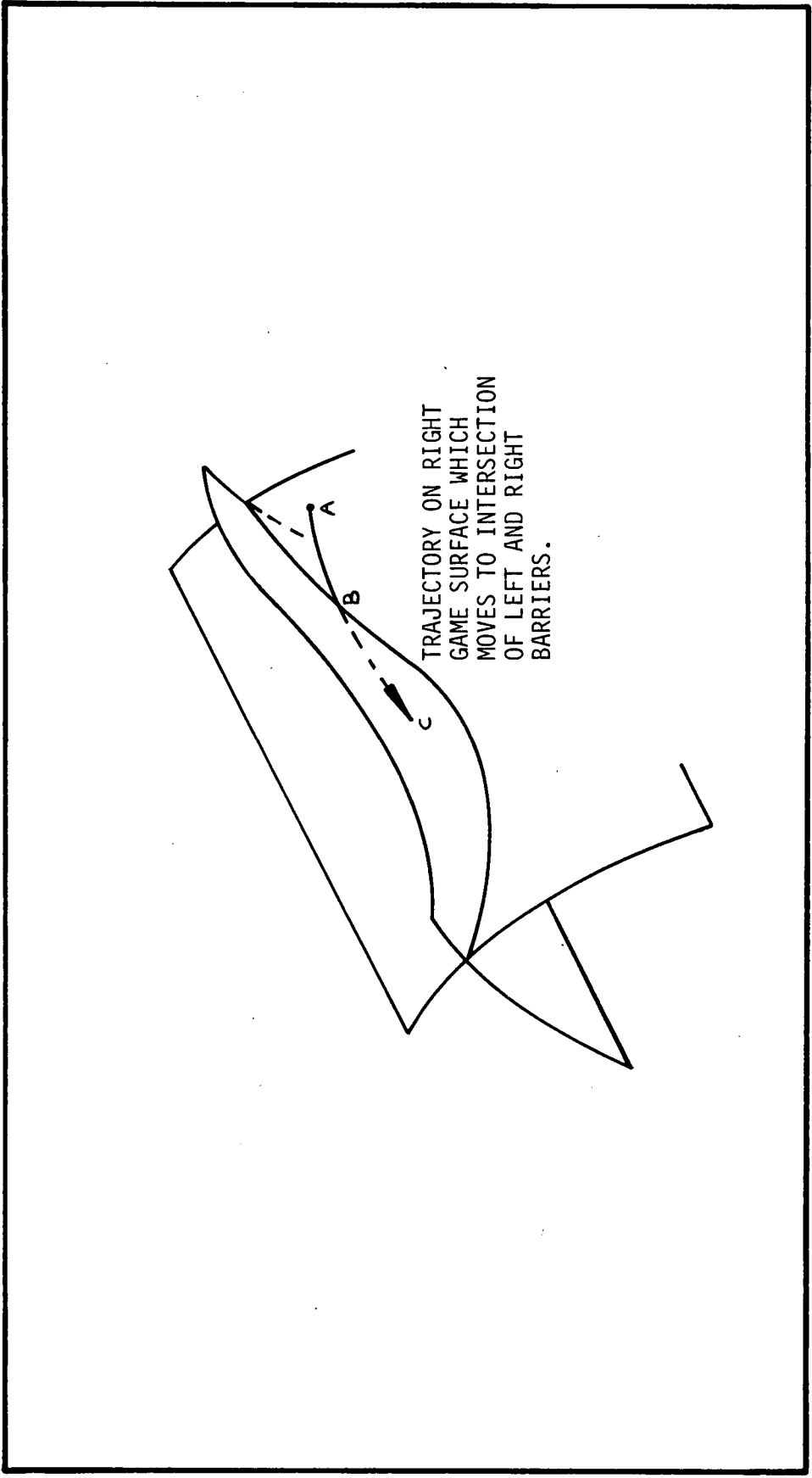


FIGURE 8 A QUALITATIVE SKETCH OF THE \overline{ABC} TRAJECTORY OF FIGURE 5

THE GREEN BARRIER - A PROBLEM IN CONTROLLABILITY

The green barrier separates the green and yellow zones. Points within the yellow zone represent states from which the pursuer can guarantee collision with the evader, provided that the evader does not perform any maneuvers. Thus the green barrier represents points controllable (by the pursuer) to the terminal set with the evader's controls set at $v = 0$ [with the system equations given by (12 - 14)].

The connection between trajectories on the boundary of controllable (or reachable sets) and abnormal trajectories for an optimal control problem has been pointed out and discussed by several authors (e.g., Ref. 3; Ref. 5, p. 350; Ref. 8, p. 206; Ref. 9, p. 138; Ref. 10, p. 41). Since we are primarily concerned with determining boundaries between various sets of points rather than specific control laws, we will avoid discussing the set up of an optimal control problem and its associated abnormal arcs. Rather we can obtain the desired boundaries directly by defining a *Controllable Surface* (similar to the game surface for the red zone) as a surface with the property that if the control u maintains a trajectory in the surface then any other admissible control must move the system either on the surface or to one side of it. This situation is depicted in Figure 9. If two such surfaces emanating from the terminal set intersect (perhaps at infinity) then the points enclosed by the terminal set and the two controllable surfaces may contain points in which the pursuer can guarantee a collision with the evader.

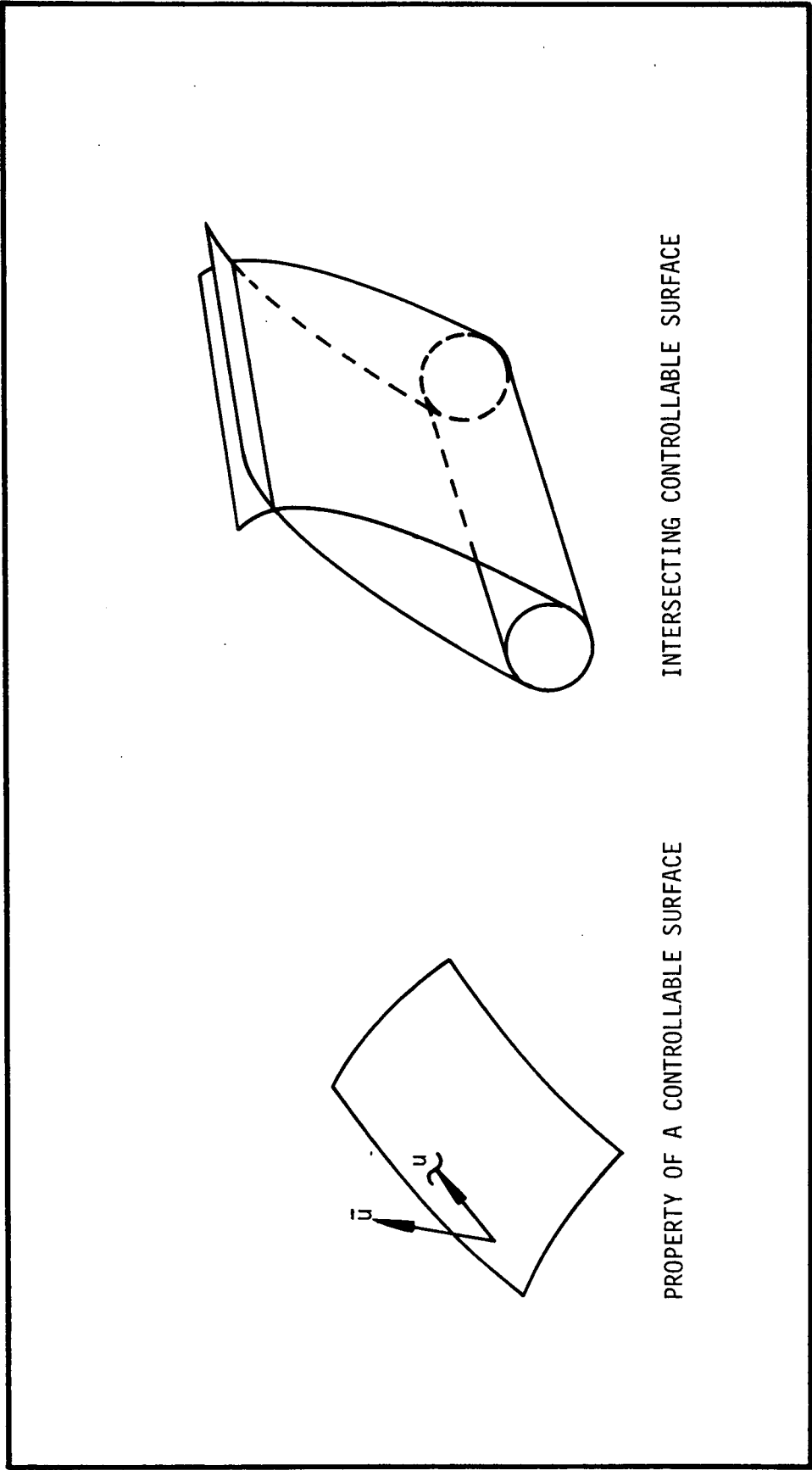


FIGURE 9 DETERMINATION OF THE GREEN BARRIER

Green Barrier Necessary Conditions

The results of references (3), (5), and (8) may be worded to apply to controllable surfaces as follows: if u is a controllable surface control for $t \in [0, t_f]$ for the dynamical system

$$\dot{\mathbf{x}} = \mathbf{f}(\mathbf{x}, u) \quad (83)$$

where $\mathbf{x}^T = [x_1 \dots x_n] \in G \subseteq E^n$, $u^T = [u_1 \dots u_r] \in U \subseteq E^r$ and where the function f is of class C^1 on $G \times U$ and if we let

$$H = \lambda^T \mathbf{f}(\mathbf{x}, u) \quad (84)$$

where $\lambda^T = [\lambda_1 \dots \lambda_n] \in E^n$, then there exists a non-zero continuous solution of the adjoint equation

$$\dot{\lambda}^T = - \frac{\partial H}{\partial \mathbf{x}} \quad (85)$$

such that for any control \bar{u} other than u

$$H(\lambda, \mathbf{x}, u) \leq H(\lambda, \mathbf{x}, \bar{u}) \quad (86)$$

$$H(\lambda, \mathbf{x}, u) = 0 \quad (87)$$

for all $t \in [0, t_f]$. Furthermore, for the problem under consideration (boundary of the yellow zone for the cylindrical collision surface) the vector λ at the terminal surface is in the direction of the outward normal to the surface.

Setting $v = 0$ in (12), (13), and (14) we obtain for H

$$H = \lambda_1 \alpha \sin x_3 + \lambda_2 (\alpha \cos x_3 - 1) - \lambda_3 u \quad (88)$$

with the adjoint system

$$\dot{\lambda}_1 = \text{constant} \quad (89)$$

$$\dot{\lambda}_2 = \text{constant} \quad (90)$$

$$\dot{\lambda}_3 = \alpha (\lambda_2 \sin x_3 - \lambda_1 \cos x_3) \quad (91)$$

Green Barrier Control

The function H is linear in u with the switching function $\sigma_u = -\lambda_3$ the same as for the red barrier analysis. The time derivatives $\dot{\sigma}_u$ and $\ddot{\sigma}_u$ are again given by (28) and (29) so that we can again conclude that singular pursuer control is given by $u = 0$. In accordance with (86) we conclude

$$u = \begin{cases} + \delta & \text{if } \sigma_u < 0 \\ - \delta & \text{if } \sigma_u > 0 \\ 0 & \text{if } \sigma_u \equiv 0 \end{cases} \quad (92)$$

The requirement on the direction of the λ vector at termination being the same as before results in the same analysis as before for the final value of the control at termination. That is, when $x_{1f} > 0$, u_f is given by (53) and $x_{1f} < 0$, u_f is given by (54).

Retrograde Integration

The controllable surfaces emanating from right and left side of the collision surface are called the right and left green barriers respectively. Trajectories which lie on these barriers are obtained by integrating the equations of motion and the adjoint equations backward from the collision surface using $v = 0$ and u control from the minimum principle (92). The initial value for u control is given by (53) and (54).

The equations for backwards integration are given by

$$\dot{x}_1(\tau) = -\alpha \sin x_3(\tau) , \quad (93)$$

$$\dot{x}_2(\tau) = -\alpha \cos x_3(\tau) + 1 , \quad (94)$$

$$\dot{x}_3(\tau) = u , \quad |u| \leq \delta , \quad (95)$$

$$\dot{\lambda}_3(\tau) = \alpha \{ \lambda_1 \cos x_3(\tau) - \lambda_2 \sin x_3(\tau) \} , \quad (96)$$

with the "initial conditions" for these equations given by (34 - 37) with the final time interpreted as an initial time.

Let $[\tau_0, \tau_s]$ be the (retro) time interval over which σ_u does not change sign, i.e., starting with $\sigma_u(\tau_0) = 0$ define

$$\tau_s \triangleq \text{first time } \sigma_u = 0 \text{ after being non-zero} . \quad (97)$$

Both Π and Π^* type of trajectories result from the backward integration. As before, the Π trajectories are obtained by integrating

the retro-equations using non-singular control on the interval $0 \leq \tau \leq \tau_s$. If τ^* is the (retro) time at which the pursuer control switches from singular to non-singular, then the Π^* trajectories are obtained by first integrating the retro-equations using singular control on the interval $0 \leq \tau \leq \tau^* \leq \tau_s$ and continuing integration using non-singular control on the interval $\tau^* \leq \tau \leq \tau_s$.

For all $\tau \in [\tau_0, \tau_s]$ $\dot{x}_3(\tau)$ is constant so that

$$\frac{d(\)}{d\tau} = u \frac{d(\)}{d x_3} . \quad (98)$$

Using this relation, the retro-equations become

$$\dot{x}_1 = - (\alpha \sin x_3) / u , \quad (99)$$

$$\dot{x}_2 = (1 - \alpha \cos x_3) / u , \quad (100)$$

$$\dot{\lambda}_3 = \alpha (\lambda_1 \cos x_3 - \lambda_2 \sin x_3) / u . \quad (101)$$

The change in (independent) variable given by (98) is subject to two constraints:

$x_3(\tau)$ must be such that $\tau \geq 0$ and

$u \neq 0$.

In particular the change in variable does not apply for u-singular control.

The Π Trajectories

Integration of equations (99 - 101) gives the non-singular trajectory (subarc) equations

$$x_1 = x_1(\tau_0) + \alpha[\cos x_3 - \cos x_3(\tau_0)]/u , \quad (102)$$

$$x_2 = x_2(\tau_0) - \alpha[\sin x_3 - \sin x_3(\tau_0)]/u + \quad (103)$$

$$[x_3 - x_3(\tau_0)]/u ,$$

and the switching function

$$\sigma_u = \alpha\{x_1(\tau_0) [\sin x_3 - \sin x_3(\tau_0)] + \quad (104)$$
$$x_2(\tau_0) [\cos x_3 - \cos x_3(\tau_0)]\}/u + \sigma_u(\tau_0) .$$

For the totally non-singular Π trajectories, we set $\sigma_u(\tau_0) = \tau_0 = 0$ and $x_1(0)$ and $x_2(0)$ are given by equations (32) and (37) with $x_{3f} = x_3(0)$.

The Π^* Trajectories

The Π^* retro-trajectories are initially u-singular and integration of equations (99 - 101) with $u = 0$ gives the u-singular (subarc) equations

$$x_1 = x_1(0) - \alpha \tau \sin x_3(0) , \quad (105)$$

$$x_2 = x_2(0) + [1 - \alpha \cos x_3(0)]\tau , \quad (106)$$

$$x_3 = x_3(0) , \quad (107)$$

and the switching function

$$\sigma_u = 0 , \quad (108)$$

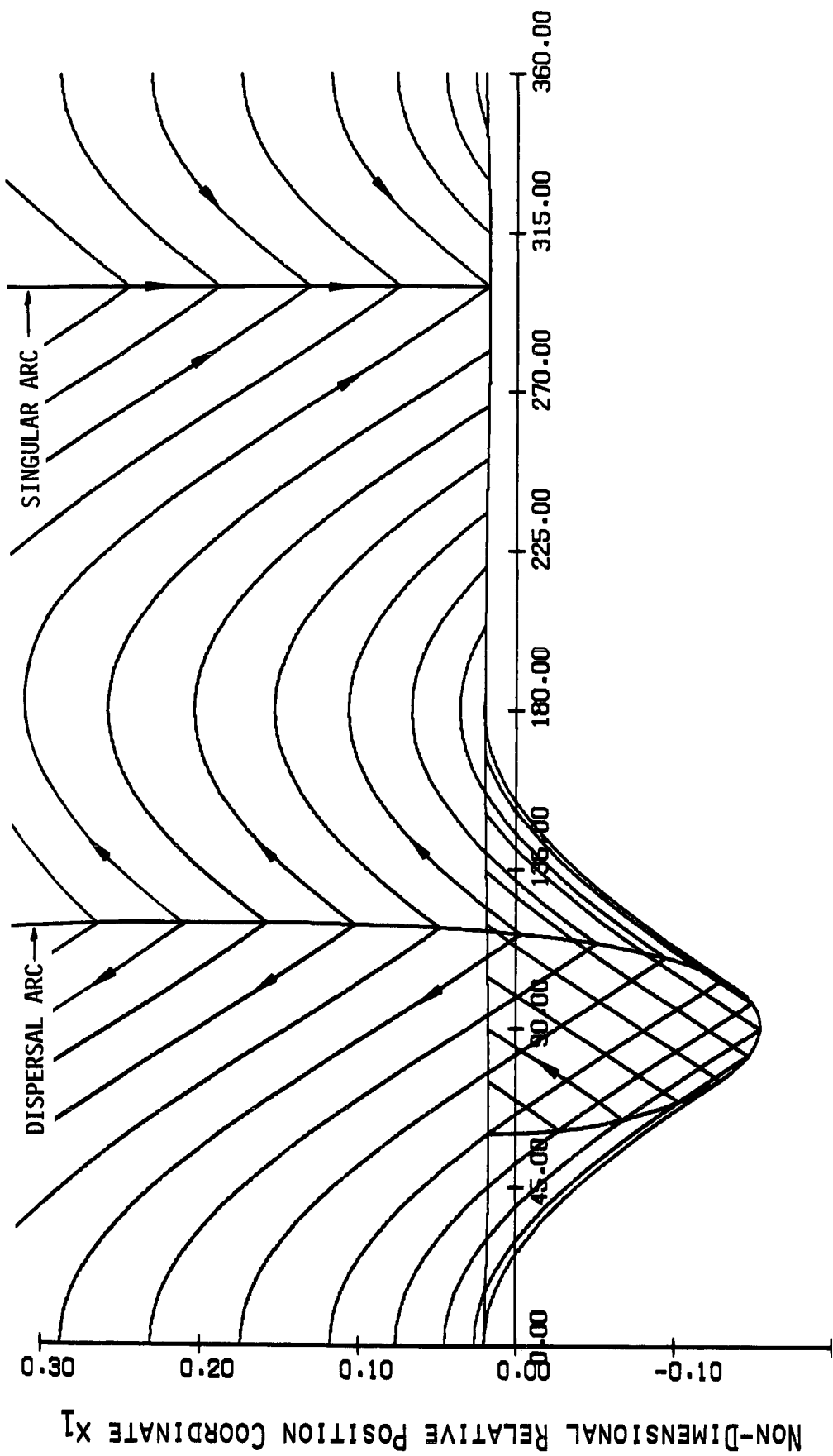
where $x_1(0)$ and $x_2(0)$ are given by equations (32) and (37) with $x_{3f} = x_3(0) = x_3^*$ on the left side $x_{3f} = x_3(0) = 2\pi - x_3^*$ on the right side.

At $\tau = \tau^*$ the pursuer switches from singular to non-singular control, and the remaining non-singular portion of the Π^* trajectory is computed from equations (102 - 104) with $\tau_0 = \tau^*$ and the "initial condition" $x_1(\tau_0)$, $x_2(\tau_0)$, $x_3(\tau_0)$, and $\sigma_u(\tau_0)$ computed from equations (105 - 108) at τ^* .

Some Observations for a Specific Case

Figures 10 and 11 show (for the case where $\alpha = 0.5$, $\delta = 2.5$, and $R = 0.02$) the projection, onto the $x_1 - x_2$ and $x_2 - x_3$ planes, of trajectories on the right portion of the green barrier. Figures 12 and 13 show the corresponding projections of the left green barrier. The dispersal curve shown is the intersection of the surface generated by trajectories which terminate (in the forward sense) at values of $x_3 > 60^\circ$, with the surface generated by trajectories which terminate with $x_3 < 60^\circ$. As before, the time to collision is discontinuous across the dispersal curve with the trajectories of least time being from

D



RELATIVE ANGLE x_3

FIGURE 10 TRAJECTORIES ON AN x_1 - x_3 PROJECTION OF THE RIGHT GREEN BARRIER

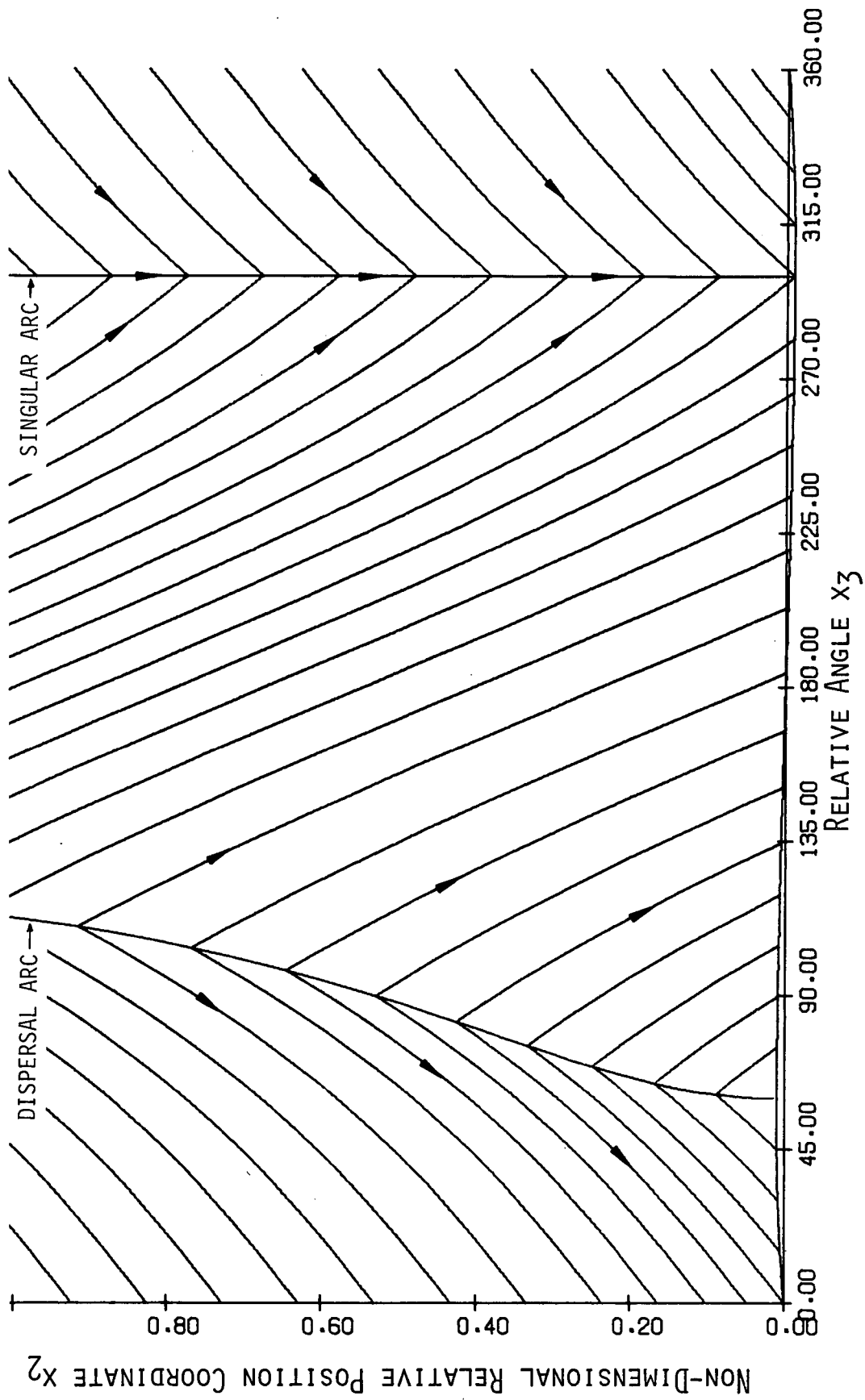
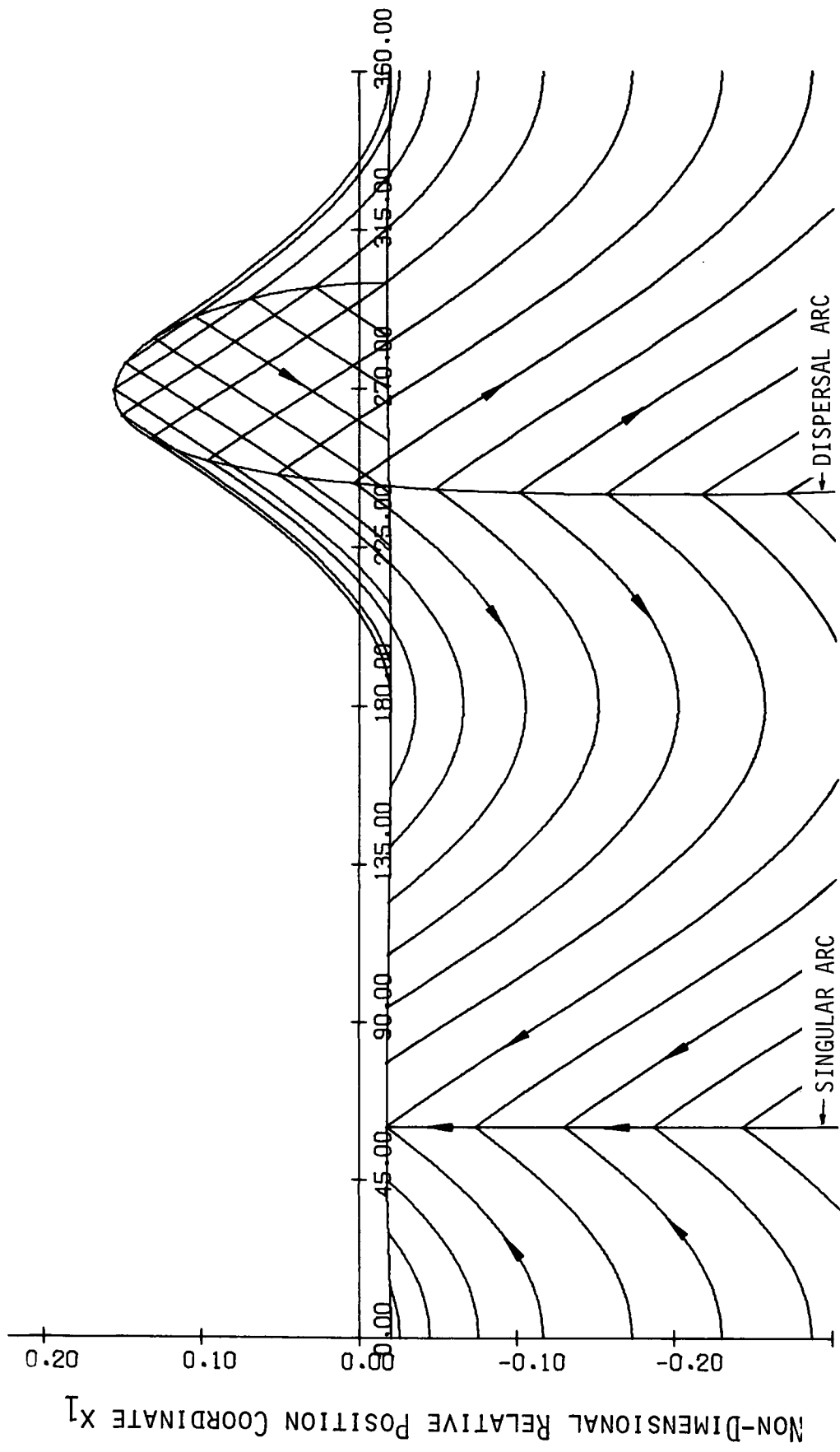


FIGURE 11 TRAJECTORIES ON AN X_2 - X_3 PROJECTION OF THE RIGHT GREEN BARRIER



RELATIVE ANGLE x_3

FIGURE 12 TRAJECTORIES ON AN x_1 - x_3 PROJECTION OF THE LEFT GREEN BARRIER

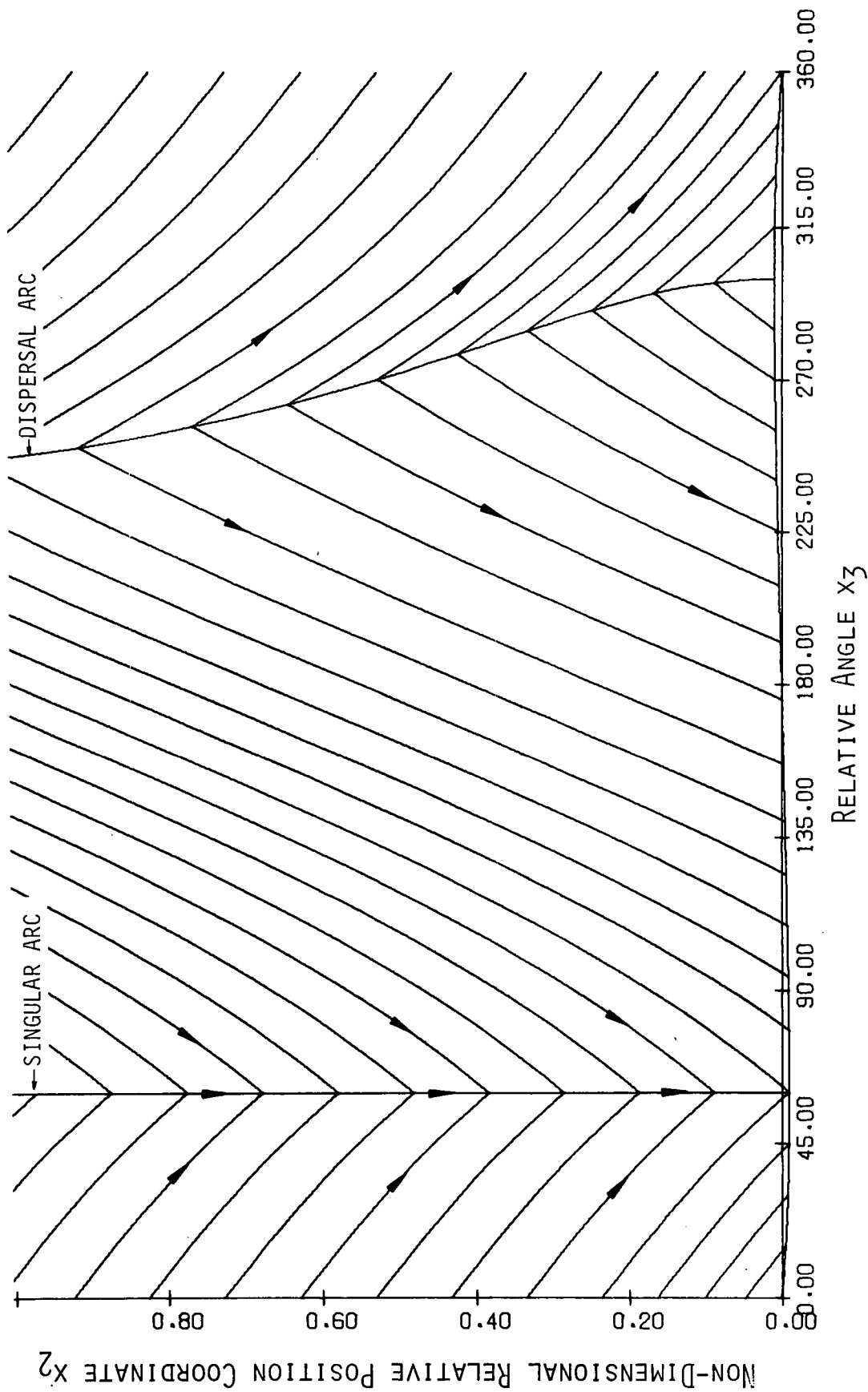


FIGURE 13 TRAJECTORIES ON AN x_2 - x_3 PROJECTION OF THE LEFT GREEN BARRIER

points on the dispersal curve terminating at values of x_3 greater than 60° .

We make the final observation that for any case, points on the green barrier do not belong to the green zone.

DISCUSSION AND ADDITIONAL RESULTS

The primary results to be presented in this section are x_3 cross-sections of the red and green barriers. A review of concepts and physical meanings will first be given.

A Review

The $x_1 - x_2 - x_3$ co-ordinate system (see Figure 1) is fixed to the evader and rotating with him in such a way that his velocity vector is always aligned with the positive x_2 axis. The positional coordinates x_1 and x_2 have been non-dimensionalized with the result that a point in the $x_1 - x_2$ plane with co-ordinates, say, $x_1 = 0$ and $x_2 = +1$ corresponds to the pursuer being directly in front of the evader at a distance equal to the evader's minimum turning radius. Such a point represents the current position of the pursuer with respect to the evader and the third coordinate, x_3 , is the clockwise angle from the evader's velocity vector. Note that x_3 is *not* the angle from the positive x_2 -axis to the *relative* velocity of the pursuer as would be seen on the evader's radar. Such a "relative heading" angle would depend not only on x_3 , the angle between the absolute velocity vectors, but also on the current turning rates of the pursuer and evader.

As previously mentioned, the $x_1 - x_2 - x_3$ state space of the system is divided into three regions which are depicted in Figure 14. They are the red zone, the yellow zone, and the green zone. The red and yellow zones are separated by a surface called the red barrier. Similarly, the yellow and green zones are separated by a (two-piece) surface called the green barrier.

A collision is said to occur when the pursuer is at or within a given radius R of the evader. This defines a "collision" surface, which is a cylinder in state space. The red barrier is constructed as the locus of game surface trajectories which terminate tangentially on the cylinder. Similarly the green barrier is constructed as the locus of controllable surface trajectories which terminate tangentially on the cylinder.

Calculation of Barrier Cross-sections

The values of the speed ratio ($\alpha = 0.5$), the turning rate ratio ($\delta = 2.5$), and the non-dimensional collision radius ($R = 0.02$) used in constructing the red and green barrier cross-sections (Figures 18 - 30) and other figures presented in this report were chosen so that a comparison with published data (Ref. 11) can be made. These parameter values are also applicable to the specific case where the evader is a Boeing 727 in a holding pattern at 230 knots and the pursuer is a Piper Comanche in an approach pattern at 110 knots. The 727's minimum turning radius (a non-dimensional distance of 1.0) for this case is about 2,400 feet so that the capture or collision circle around the evader has a

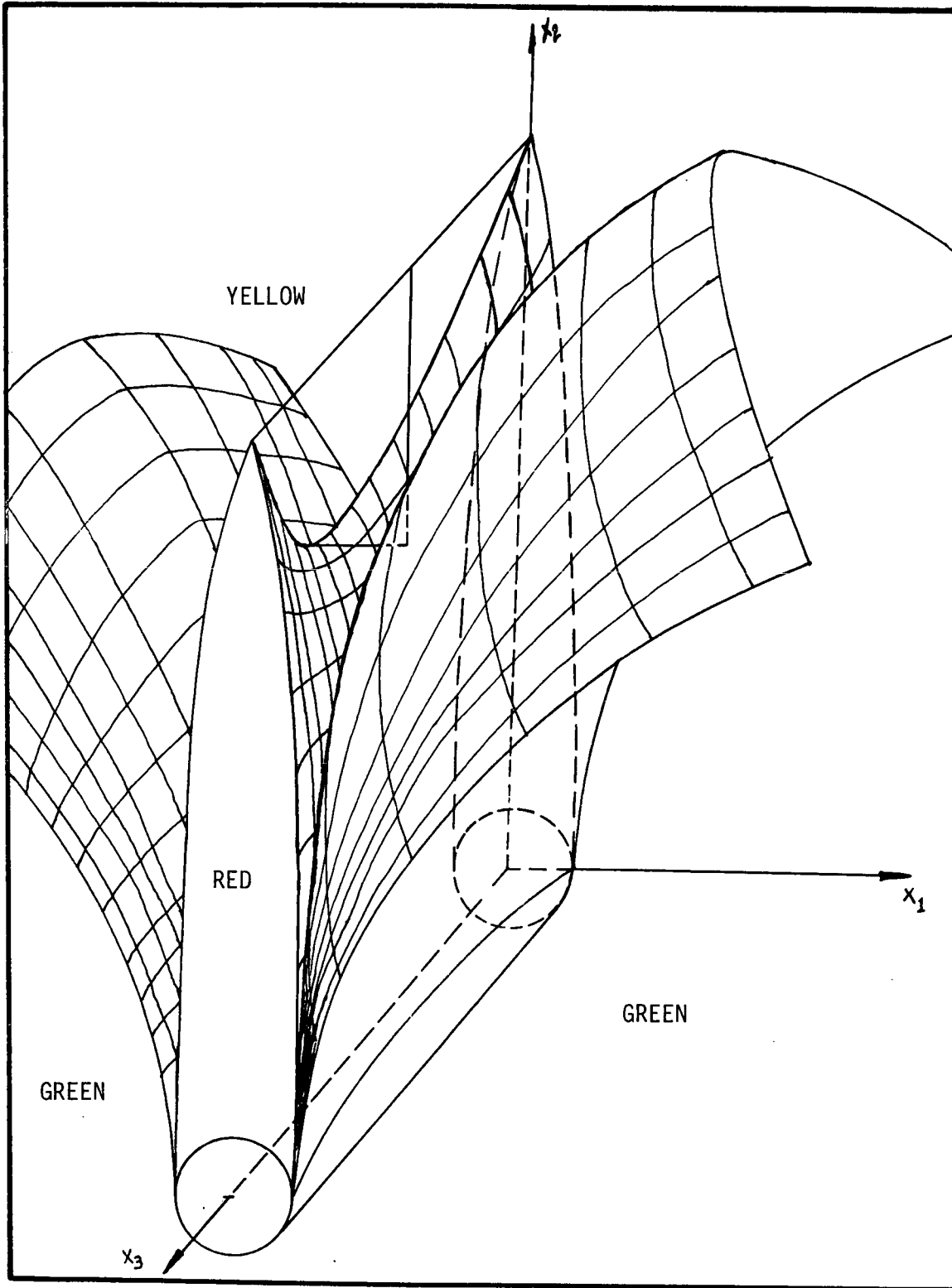


FIGURE 14 A QUALITATIVE SKETCH OF THE RED AND GREEN BARRIERS

diameter of about 100 feet, i.e., slightly less than the wing span of the 727.

Although the red and green barriers have many similarities, the left and right green barriers, where the evader's turning rate is everywhere zero, are geometrically "nicer" surfaces than their red barrier counterparts. Figure 15 shows a sketch of the three dimensional right green barrier. Regions I and III are "curved" (differently), but regions II and IV are planar. These planes intersect along the dispersal arc and along the $x_3 = 300^\circ$ singular arc.

This planar phenomenon occurs on the left green barrier as well as on the right, but it does not occur anywhere on the red barrier. It is a direct consequence of the fact that the evader executes straight line motion on the green barrier thus enabling the pursuer, if he is "far enough ahead" of the evader, to come to a constant-line-of-sight collision course heading in which both aircraft fly in straight lines. This situation does not occur on the red barrier where the evader is always turning to avoid a collision.

As an example of a collision encounter, consider the case where the pursuer is initially on the right green barrier in Region I (Point A, Figure 15) at a heading of $x_3 = 120^\circ$ with respect to the evader. The evader, by hypothesis, does not attempt to avoid a collision and remains on his initial course and heading while the pursuer executes a hard right turn. Because the pursuer starts on the green barrier, the encounter ends tangentially, that is, the pursuer's

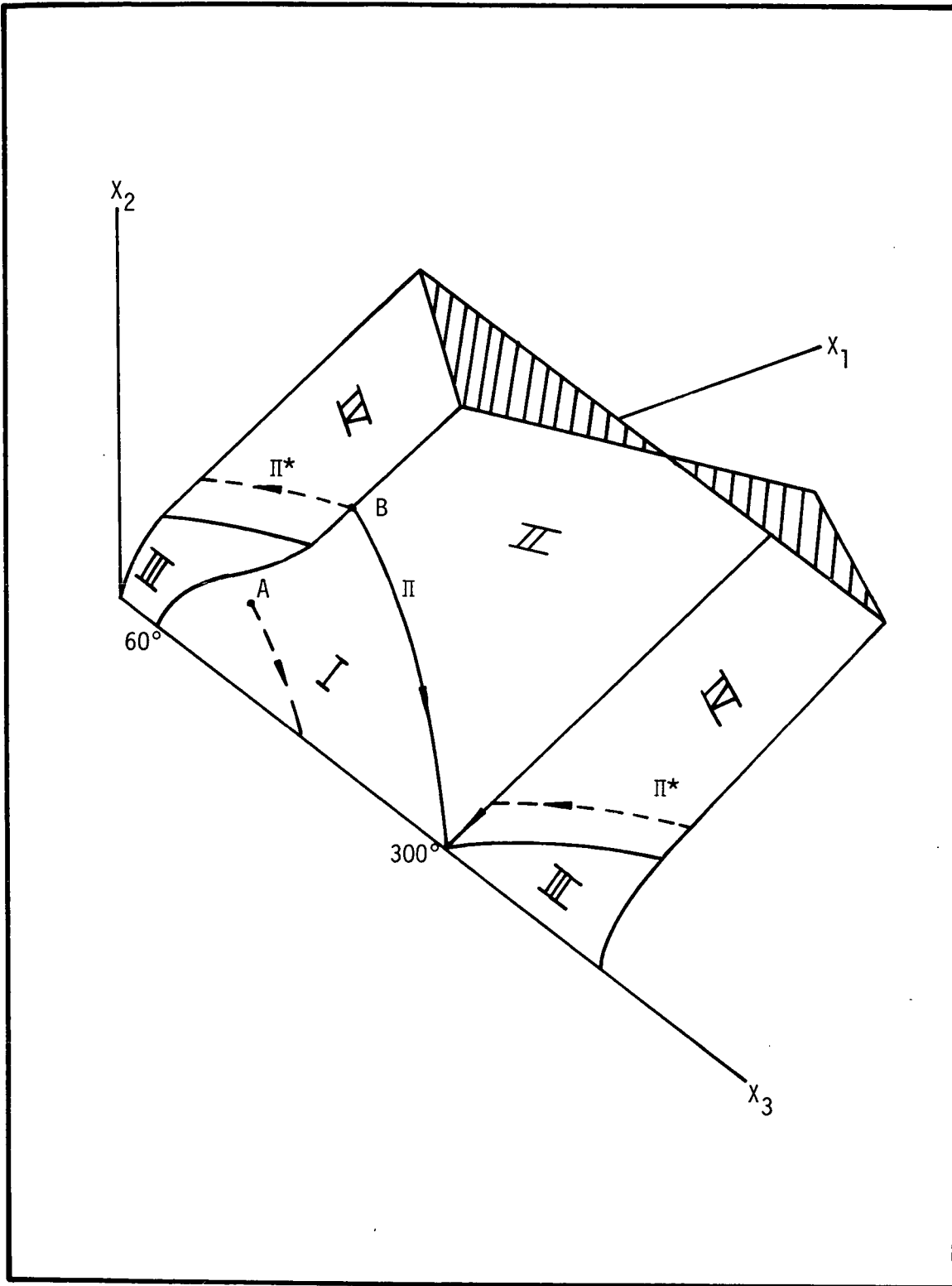


FIGURE 15 A QUALITATIVE SKETCH OF THE RIGHT GREEN BARRIER

trajectory is tangent to the collision surface at the point of contact. Figure 16 shows the resulting trajectory as seen on the evader's radar. Note that the pursuer's velocity vector is *not* tangent to the radar trajectory, i.e., x_3 is not the relative heading angle as seen on the evader's radar, but the clockwise angle from the evader's absolute velocity vector (the positive x_2 - axis) to the pursuer's absolute velocity vector. Also note that each point on the trajectory corresponds to a different value of x_3 . Therefore, at each instant of time the appropriate green barrier cross-section is continuously changing with the result that the evader can *not* observe the entire encounter by charting the motion of the pursuer with respect to only one barrier cross-section.

From initial positions on the right green barrier in Region I, as in the previous example, or in Region III, the pursuer executes a hard right- or left-hand turn, respectively, and the collision occurs tangentially while the pursuer is still in the turn. If, on the other hand, the initial state of the system is on the right green barrier in Regions II or IV, the pursuer executes a hard right or left turn, respectively, until he comes to a heading of $x_3 = 300^\circ$. He then maintains this heading until the collision occurs. Figure 17 shows a typical trajectory from Region II as seen on the evader's radar.

At this point the exact nature of the discontinuity in the time to collision across a dispersal curve can be clarified. Consider the trajectory, (Π in Figure 15) on the right green barrier, which terminates at $x_3 = 300^\circ$ and separates Region I and II. This trajectory

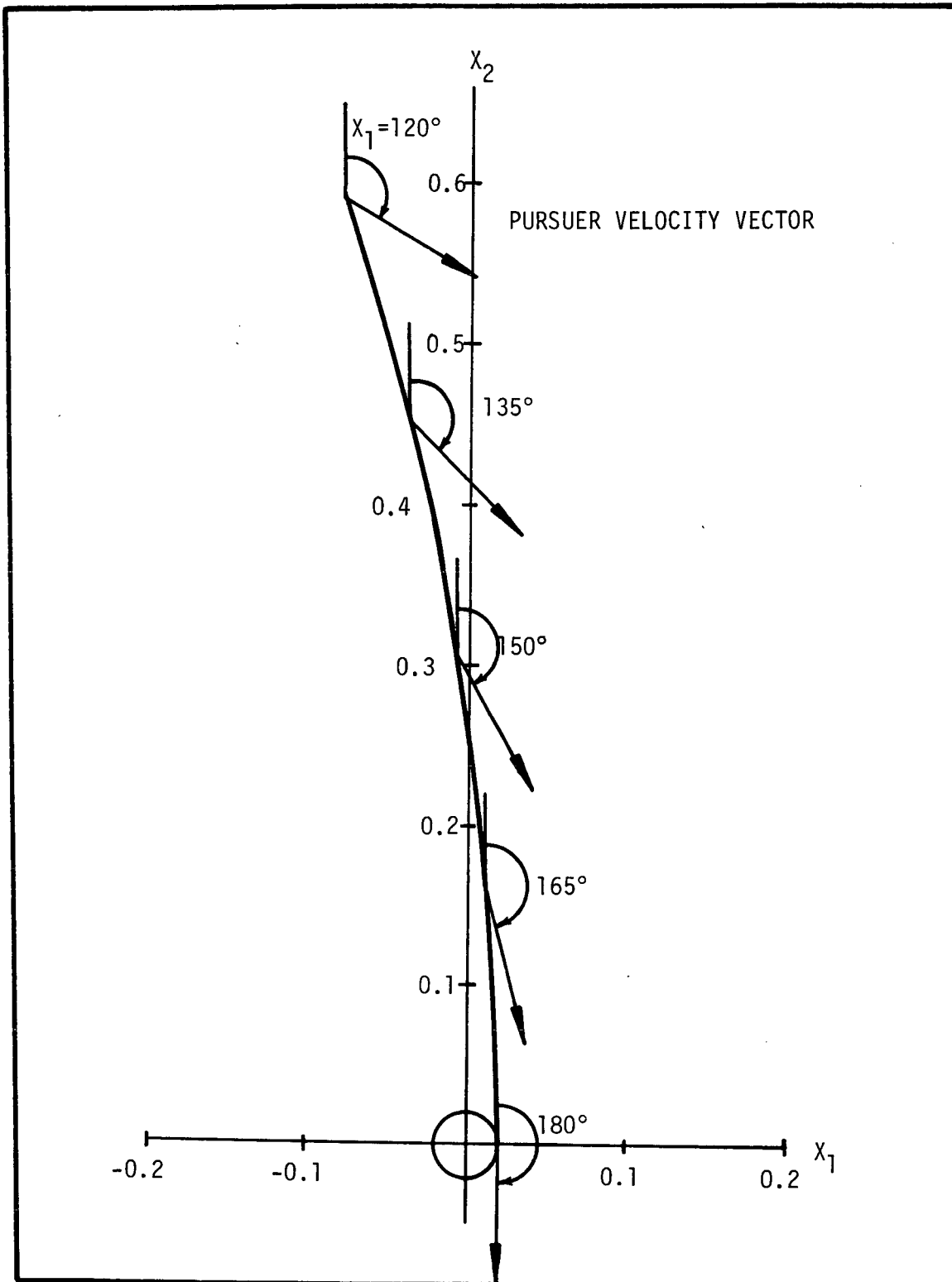


FIGURE 16 A REGION I RIGHT GREEN BARRIER COLLISION ENCOUNTER SEEN ON EVADER'S RADAR

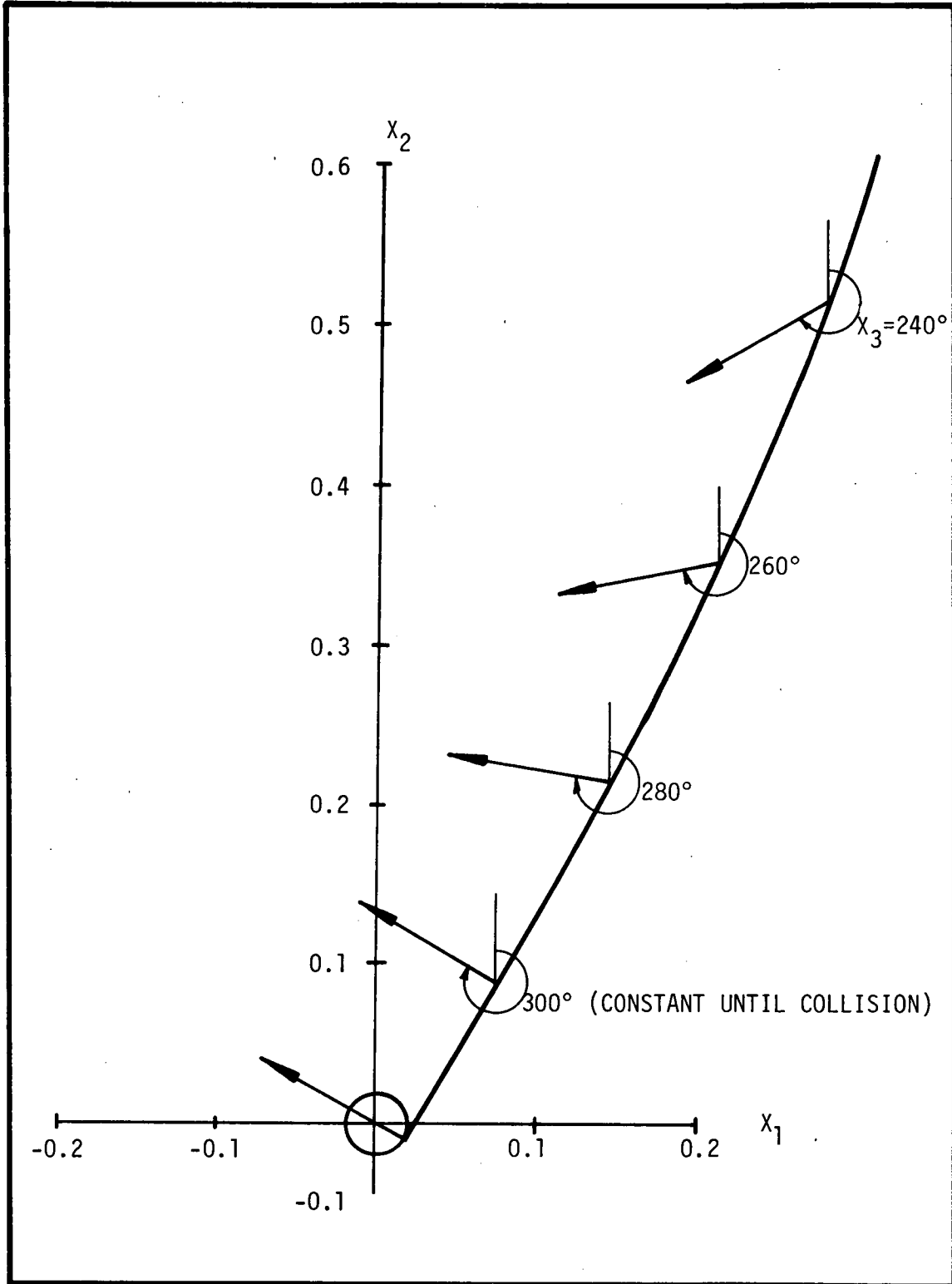


FIGURE 17 A REGION II RIGHT GREEN BARRIER COLLISION ENCOUNTER SEEN ON EVADER'S RADAR

may be thought of as starting from the point where it intersects the dispersal curve. Also consider the Region IV trajectory (Π^* in Figure 15) starting from this same point. Along the Π trajectory the pursuer executes a hard right turn ($u = -\delta$) until he comes to a heading of $x_3 = 300^\circ$. At that instant the collision occurs. The elapsed non-dimensional time is given by equation (95) as approximately π/δ ($\Delta x_3 \cong 180^\circ$). On the other hand the Region IV trajectory requires approximately the same amount of time just to reach the $x_3 = -60^\circ$ (300°) singular arc heading. The pursuer must then consume additional time flying at this heading before the collision occurs.

The dispersal curves on the left- and right-hand portions of the red and green barriers, in addition to being curves across which the time to collision is discontinuous, are also loci of points where retro trajectories using barrier control would leave the barriers. For example, consider the right green barrier trajectory Π in Region I (Figure 15) which terminates at $x_3 = 300^\circ$. If the trajectory is traversed in the opposite direction, by integrating the equations of motion backwards from the collision surface, point B on the dispersal curve will be reached. This portion of the trajectory lies entirely on the right green barrier. If the backwards integration is continued beyond the dispersal curve, the trajectory will leave the barrier and enter the yellow zone.

Barrier Cross-section

Figures 18 - 30 are x_3 -cross-sections of the state space, showing the red, yellow, and green zones and the red and green barriers separating them, for values of x_3 ranging from $x_3 = 0^\circ$ to $x_3 = 180^\circ$ in 15° increments. Figure 31 shows the barrier cross-sections at $x_3 = 270^\circ$ ($180^\circ + 90^\circ$) for a comparison of this figure with the $x_3 = 90^\circ$ cross-section. Any cross-section at $x_3 = 180^\circ + \gamma$ can be obtained from the cross-section at $x_3 = 180^\circ - \gamma$ by replacing x_1 by $-x_1$.

Examination of Results

Examination of the 0° and 180° cross-sections (Figures 18 and 30) reveals that the horizontal distance from the x_2 axis to the barrier in both cases increases along the x_2 axis, reaches a maximum, and then decreases until the right and left red barriers intersect. In addition the maximum width is of the same magnitude for both of these red barriers. This "bulge" in the red barrier is best understood by considering the expanding nature of the $x_3 = 0^\circ$ green barrier cross-section (Figure 18).

Suppose the pursuer is initially in the green zone on the x_1 axis slightly to the left of the collision surface, say at $x_1 = -0.15$, and moving in the same direction as the evader. Let the pursuer execute a hard right turn in an attempt to cause a collision and let the evader, the faster but less maneuverable of the two aircraft, continue in straight line motion. By the time the pursuer's turn brings him to the x_2 -axis, he will be behind the faster evader and no collision will

E

NON-DIMENSIONAL RELATIVE POSITION COORDINATE x_2

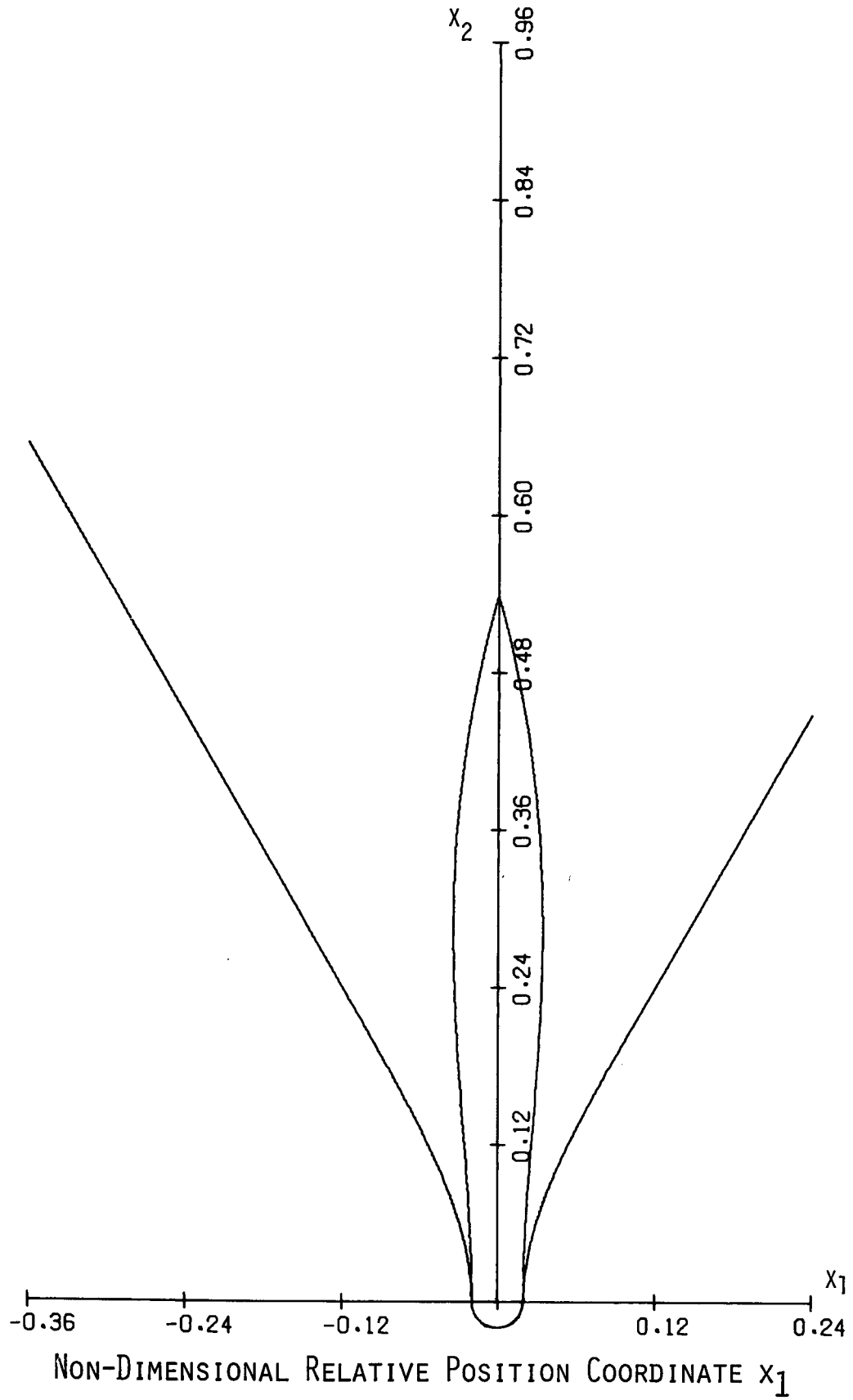


FIGURE 18 RED AND GREEN BARRIER CROSS SECTION AT $x_3=0^\circ$

NON-DIMENSIONAL RELATIVE POSITION COORDINATE x_2

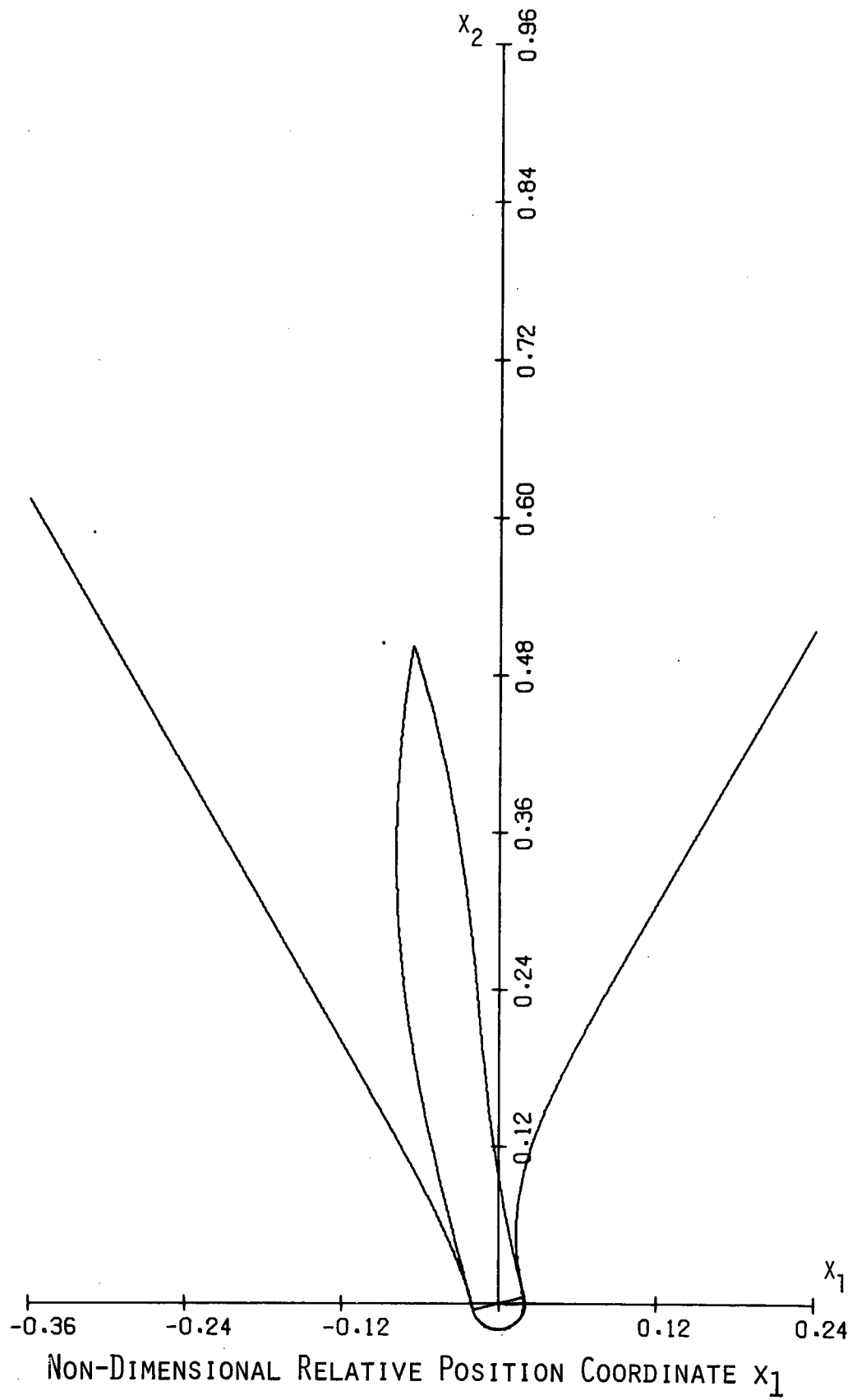


FIGURE 19 RED AND GREEN BARRIER CROSS SECTION AT $x_3=15^\circ$

NON-DIMENSIONAL RELATIVE POSITION COORDINATE x_2

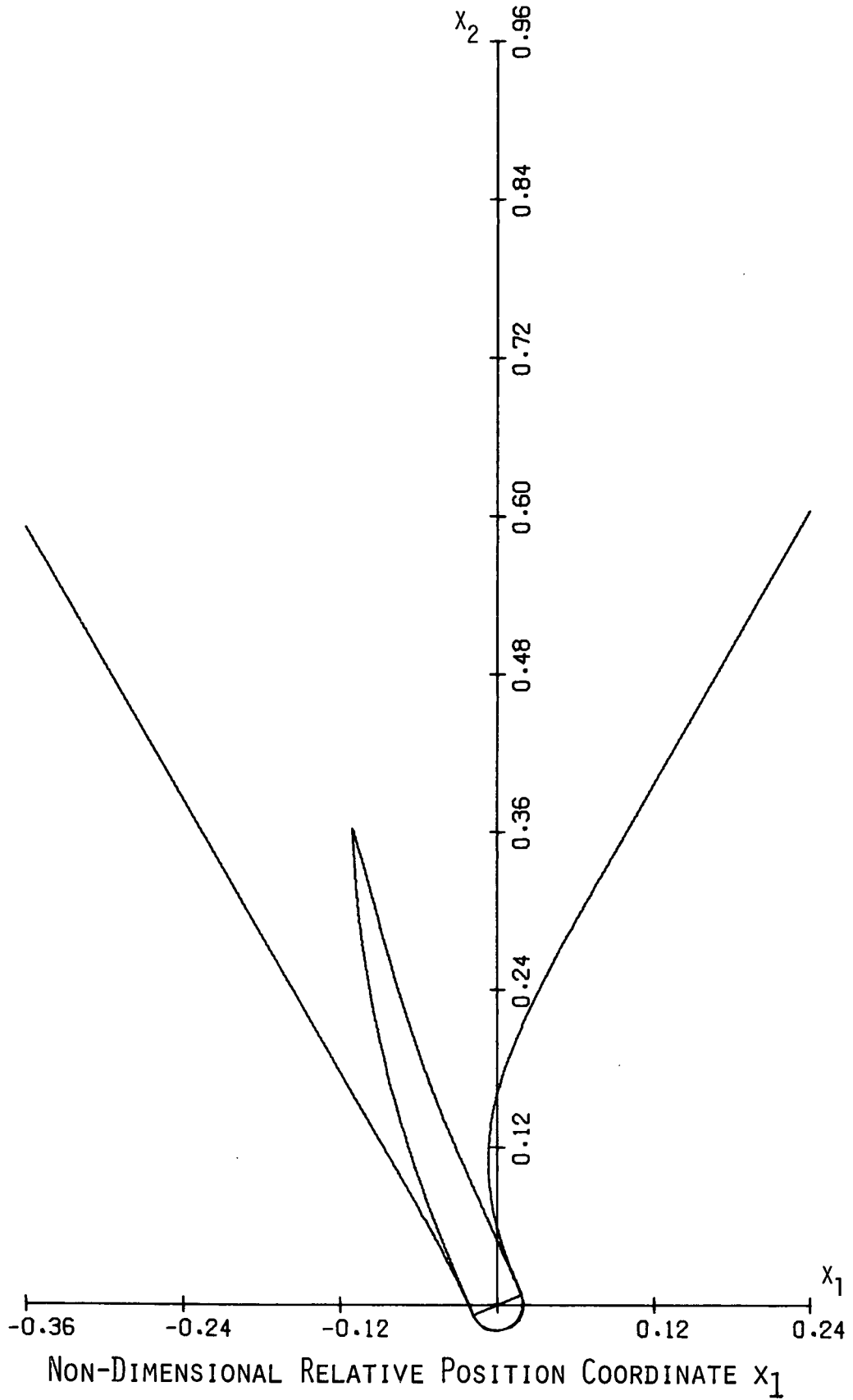


FIGURE 20 RED AND GREEN BARRIER CROSS SECTION AT $x_3=30^\circ$

NON-DIMENSIONAL RELATIVE POSITION COORDINATE x_2

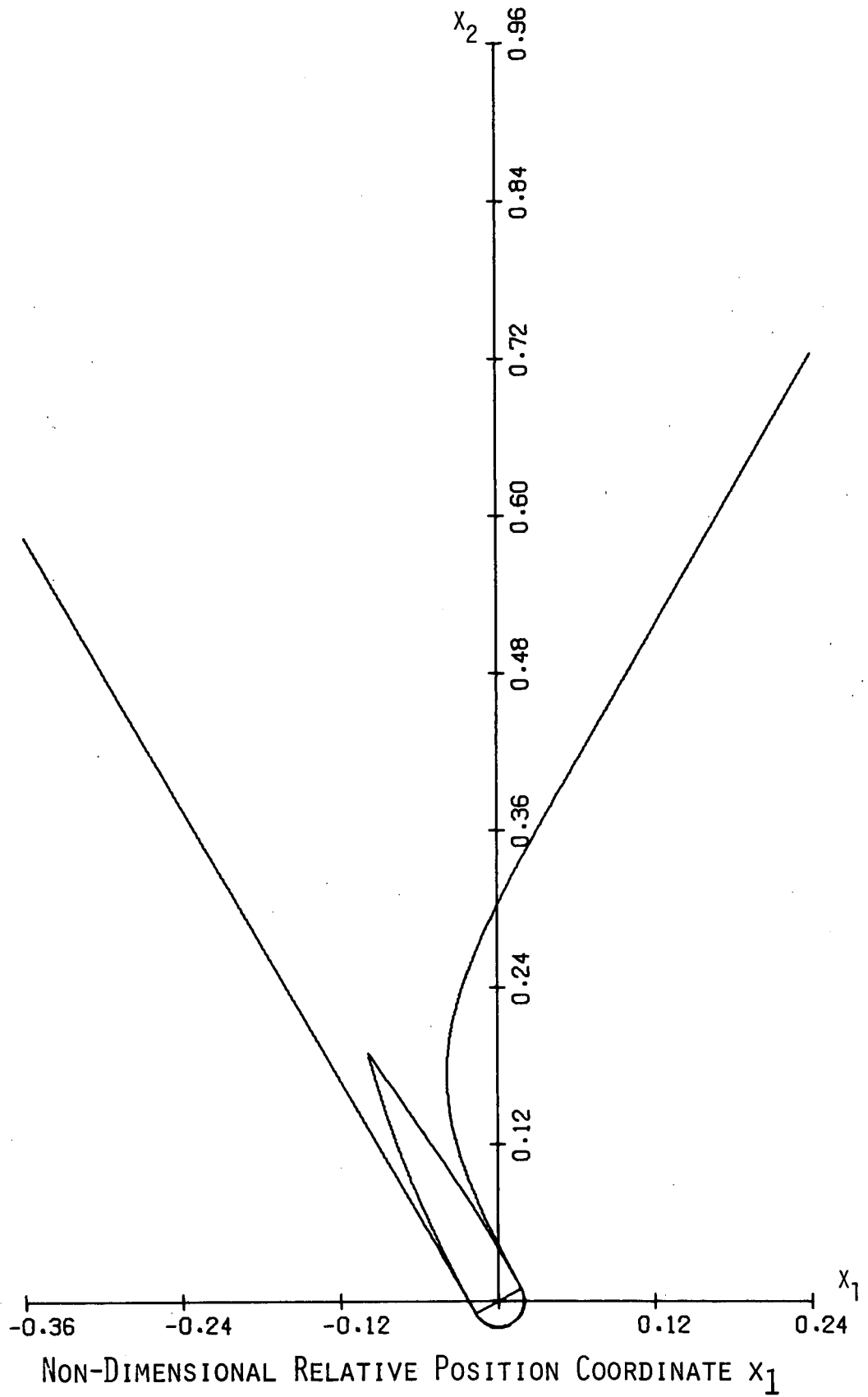


FIGURE 21 RED AND GREEN BARRIER CROSS SECTION AT $x_3=45^\circ$

NON-DIMENSIONAL RELATIVE POSITION COORDINATE x_2

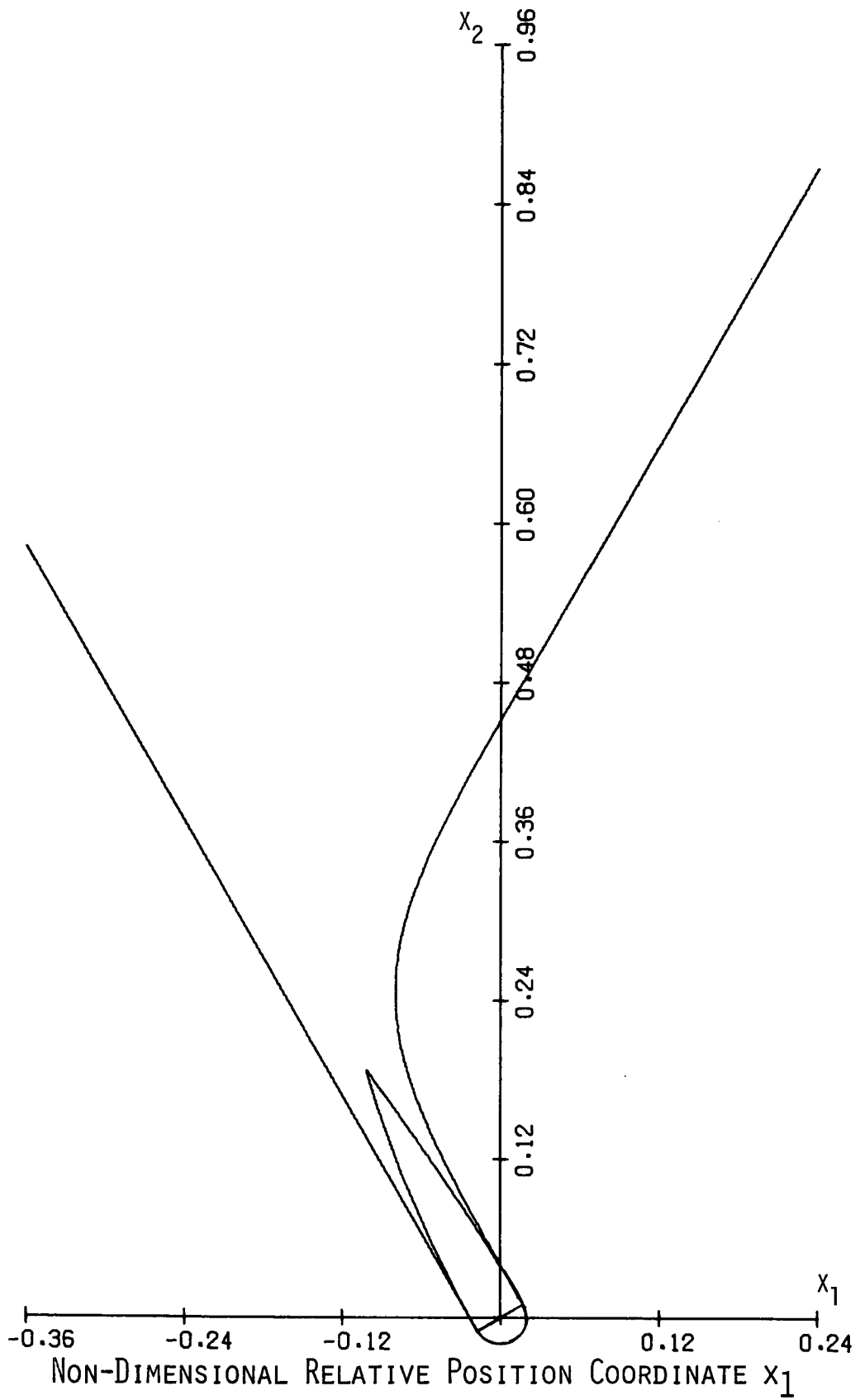


FIGURE 22 RED AND GREEN BARRIER CROSS SECTION AT $x_3=60^\circ$

NON-DIMENSIONAL RELATIVE POSITION COORDINATE x_2

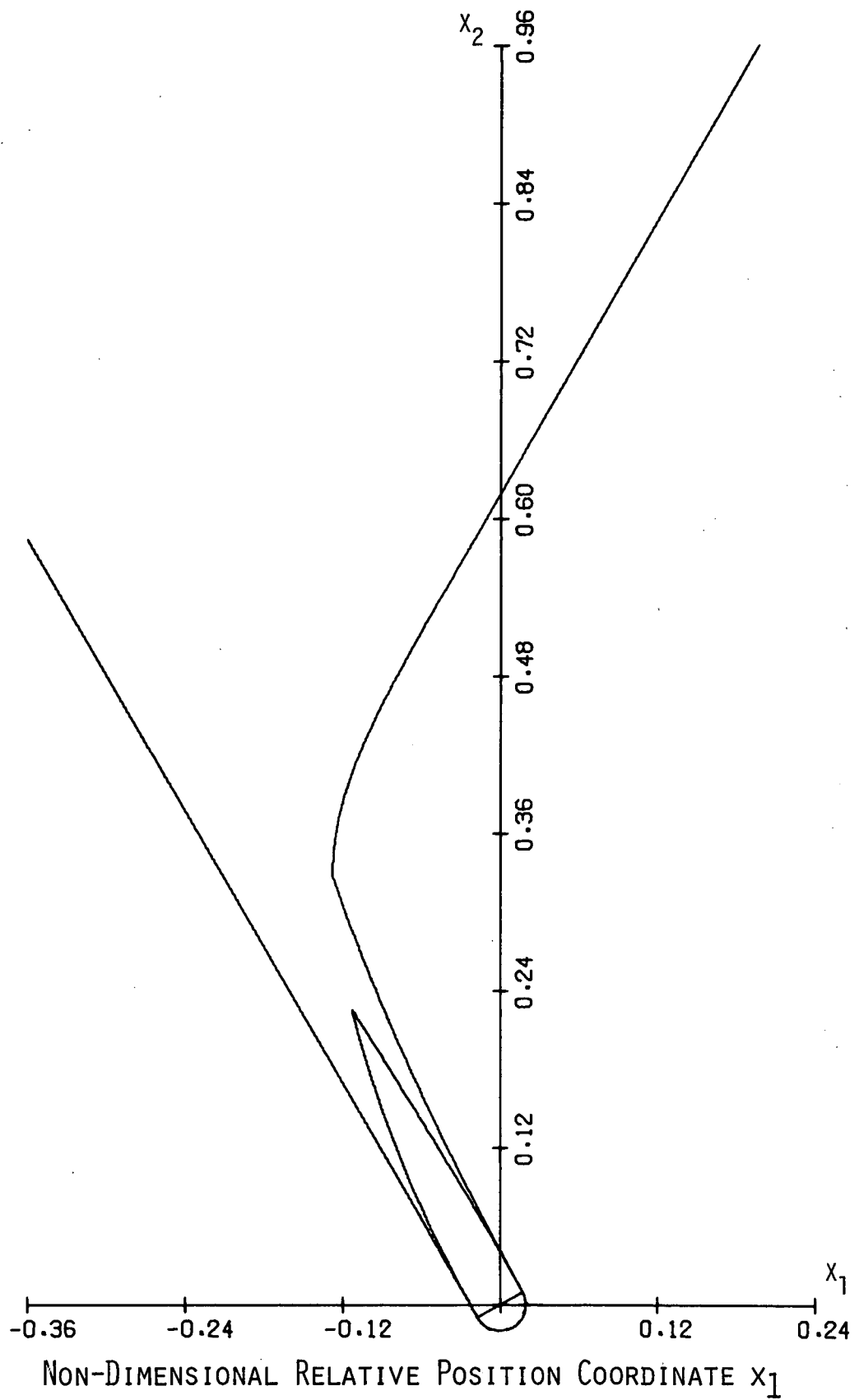


FIGURE 23 RED AND GREEN BARRIER CROSS SECTION AT $x_3=75^\circ$

NON-DIMENSIONAL RELATIVE POSITION COORDINATE x_2

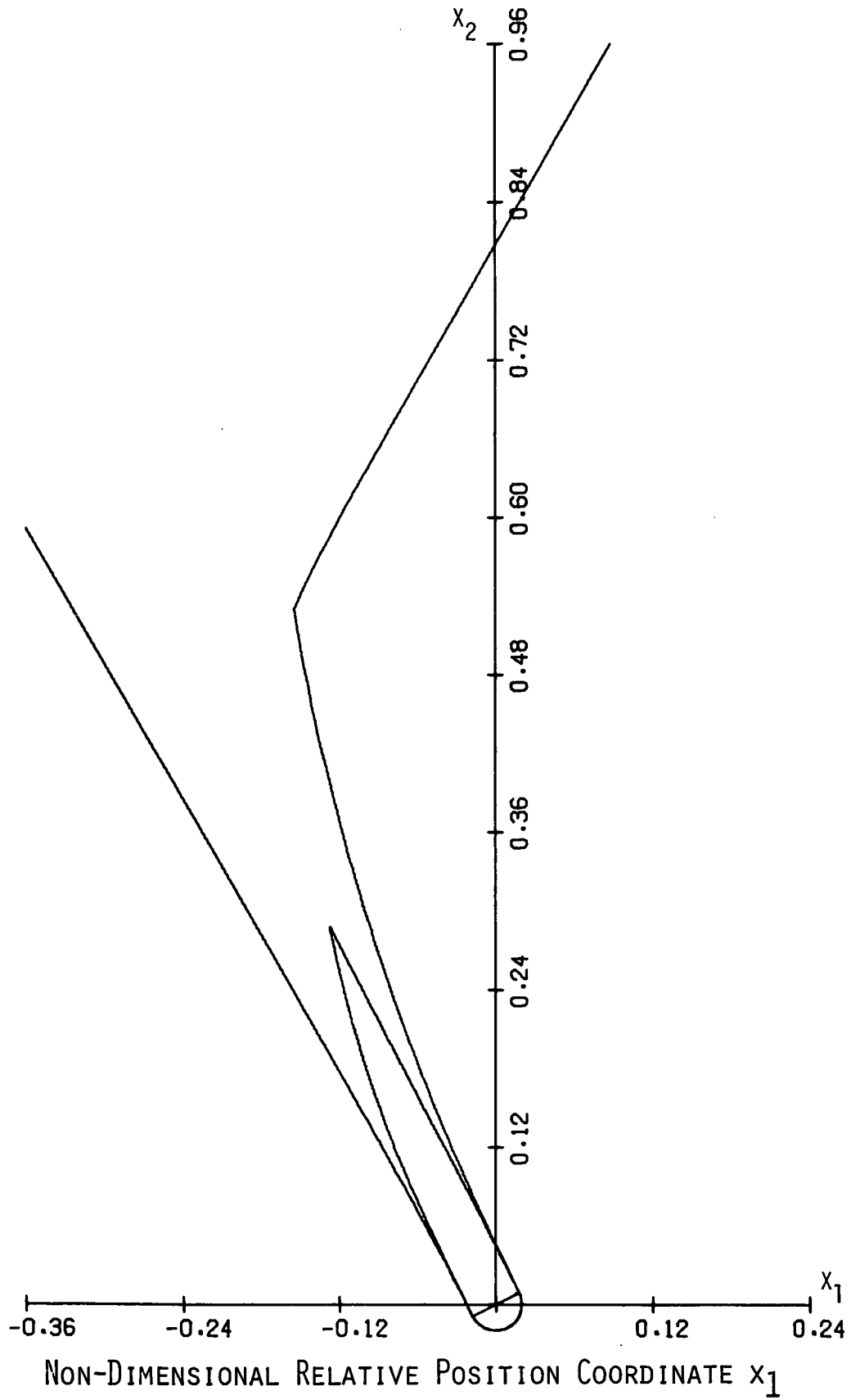


FIGURE 24 RED AND GREEN BARRIER CROSS SECTION AT $x_3=90^\circ$

NON-DIMENSIONAL RELATIVE POSITION COORDINATE x_2

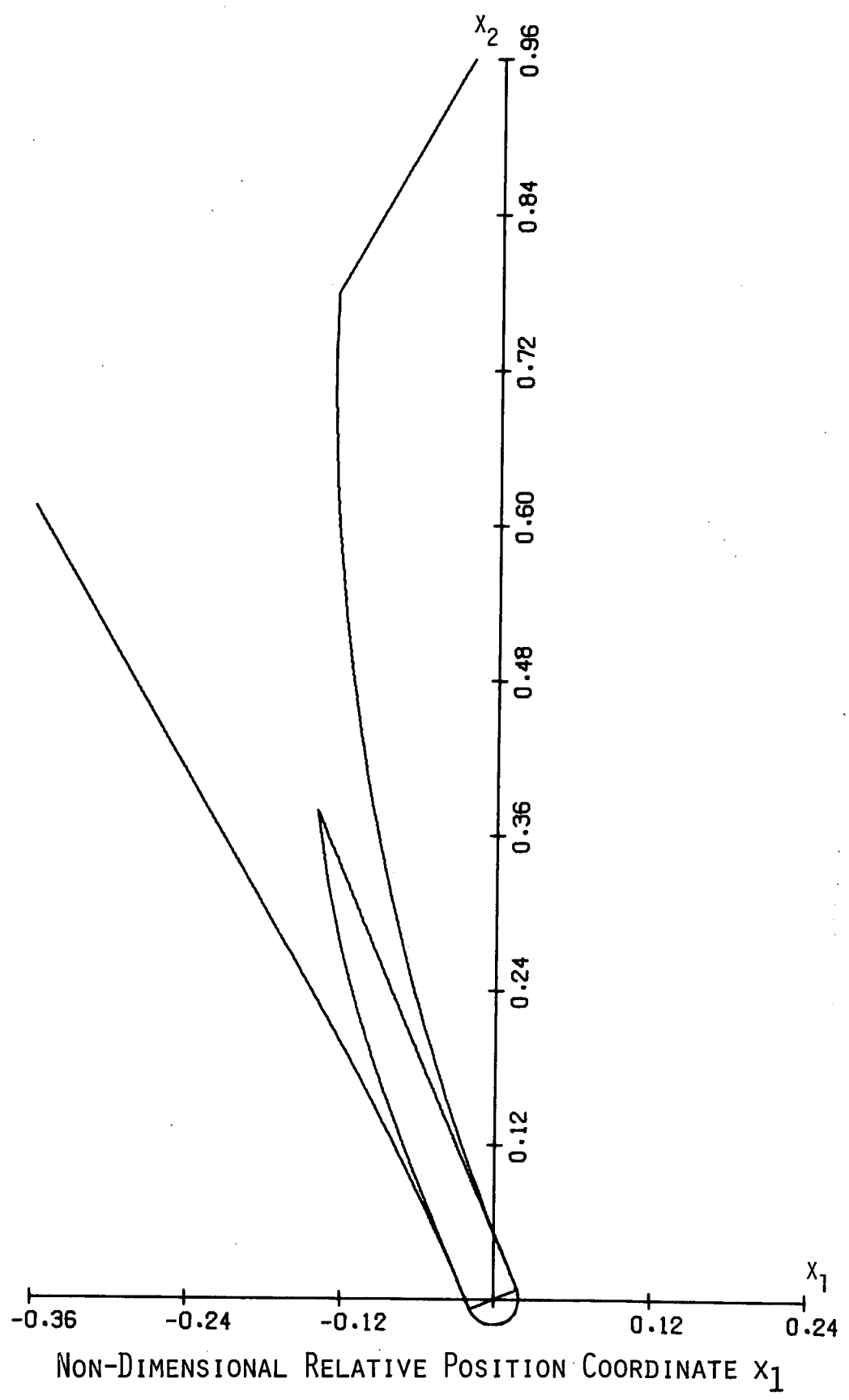


FIGURE 25 RED AND GREEN BARRIER CROSS SECTION AT $x_3=105^\circ$

NON-DIMENSIONAL RELATIVE POSITION COORDINATE x_2

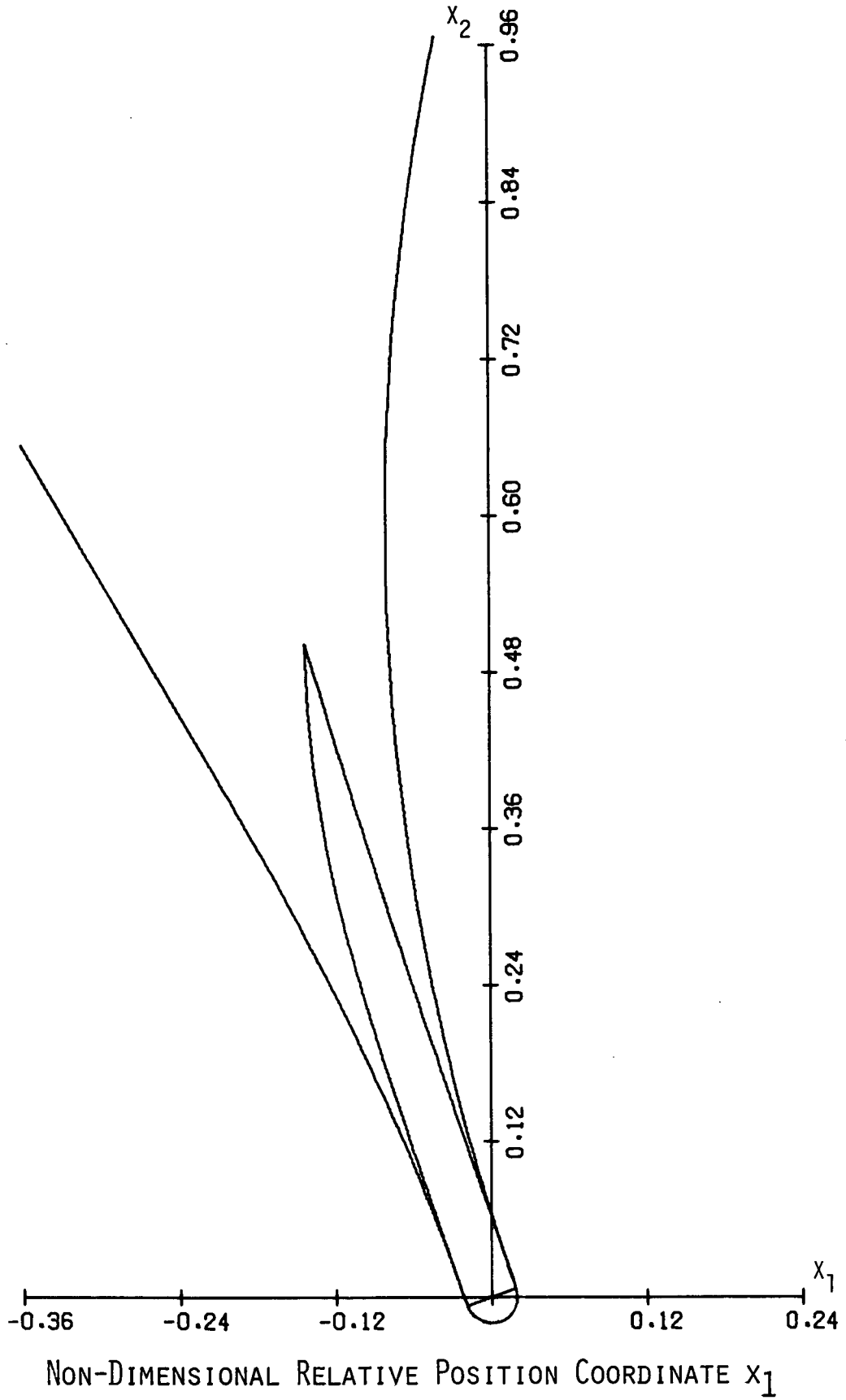


FIGURE 26 RED AND GREEN BARRIER CROSS SECTION AT $x_3=120^\circ$

NON-DIMENSIONAL RELATIVE POSITION COORDINATE x_2

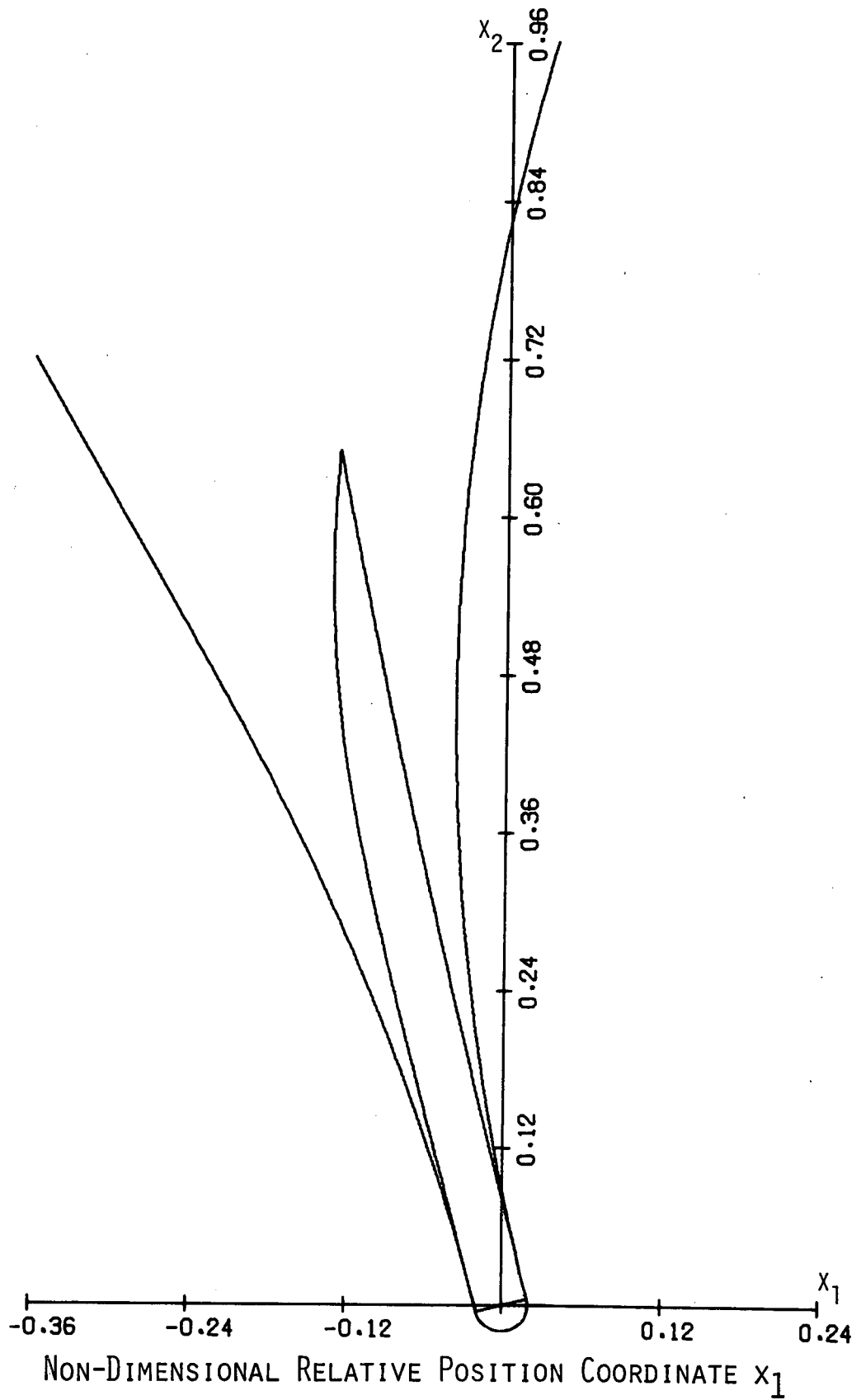


FIGURE 27 RED AND GREEN BARRIER CROSS SECTION AT $x_3=135^\circ$

NON-DIMENSIONAL RELATIVE POSITION COORDINATE x_2



FIGURE 28 RED AND GREEN BARRIER CROSS SECTION AT $x_3=150^\circ$

NON-DIMENSIONAL RELATIVE POSITION COORDINATE x_2

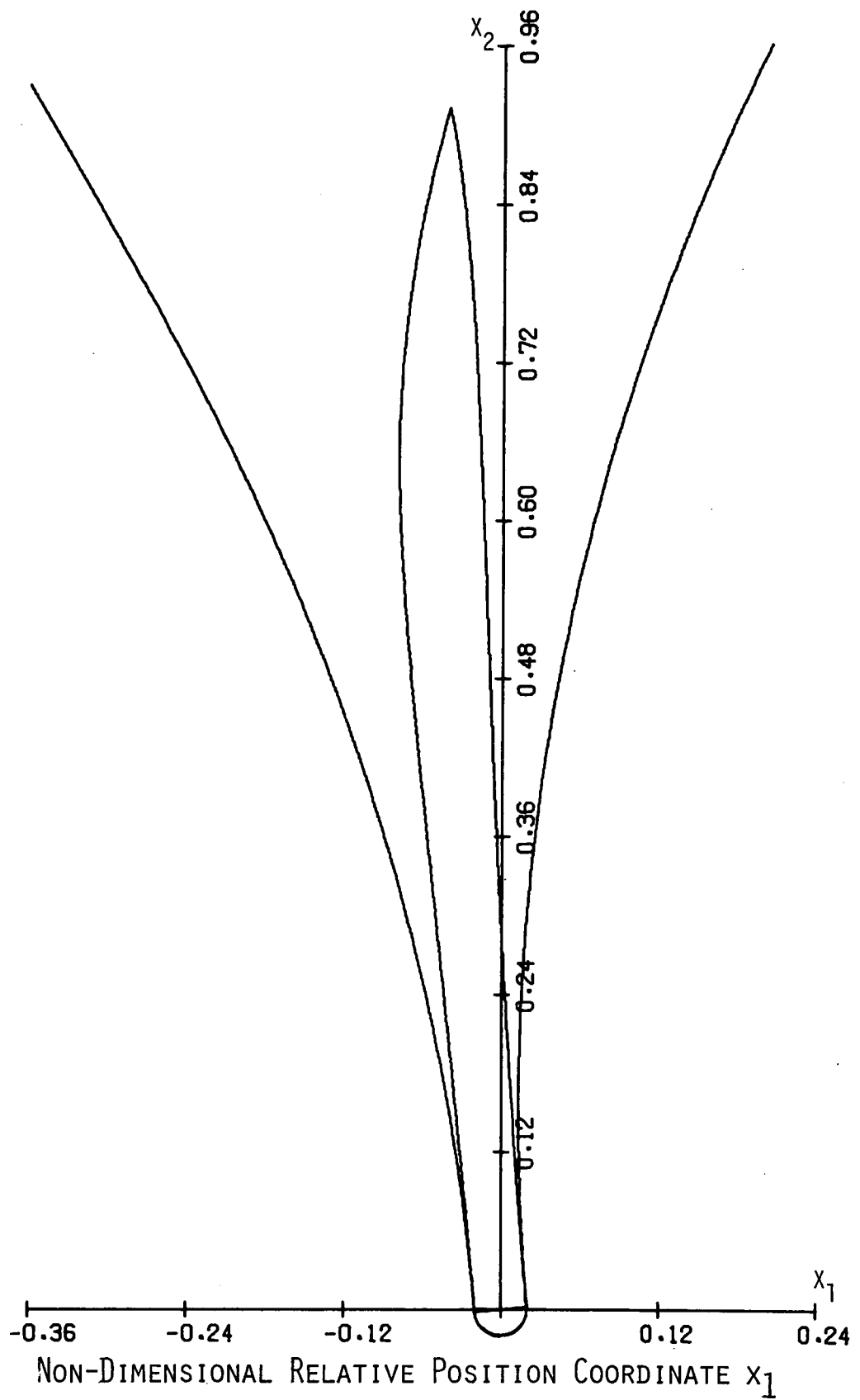


FIGURE 29. RED AND GREEN BARRIER CROSS SECTION AT $x_3=165^\circ$

NON-DIMENSIONAL RELATIVE POSITION COORDINATE x_2

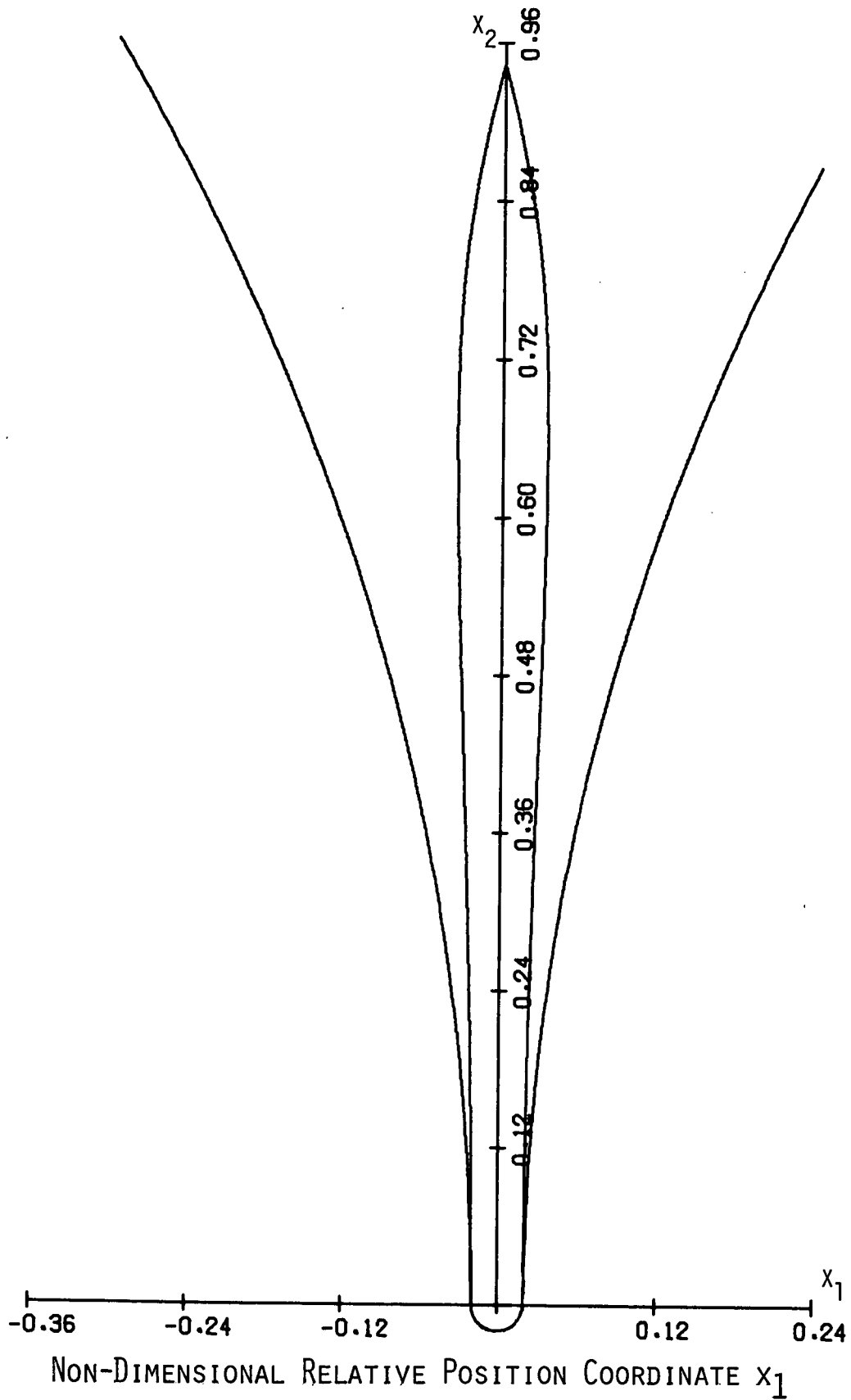


FIGURE 30 RED AND GREEN BARRIER CROSS SECTION AT $x_3=180^\circ$

NON-DIMENSIONAL RELATIVE POSITION COORDINATE x_2

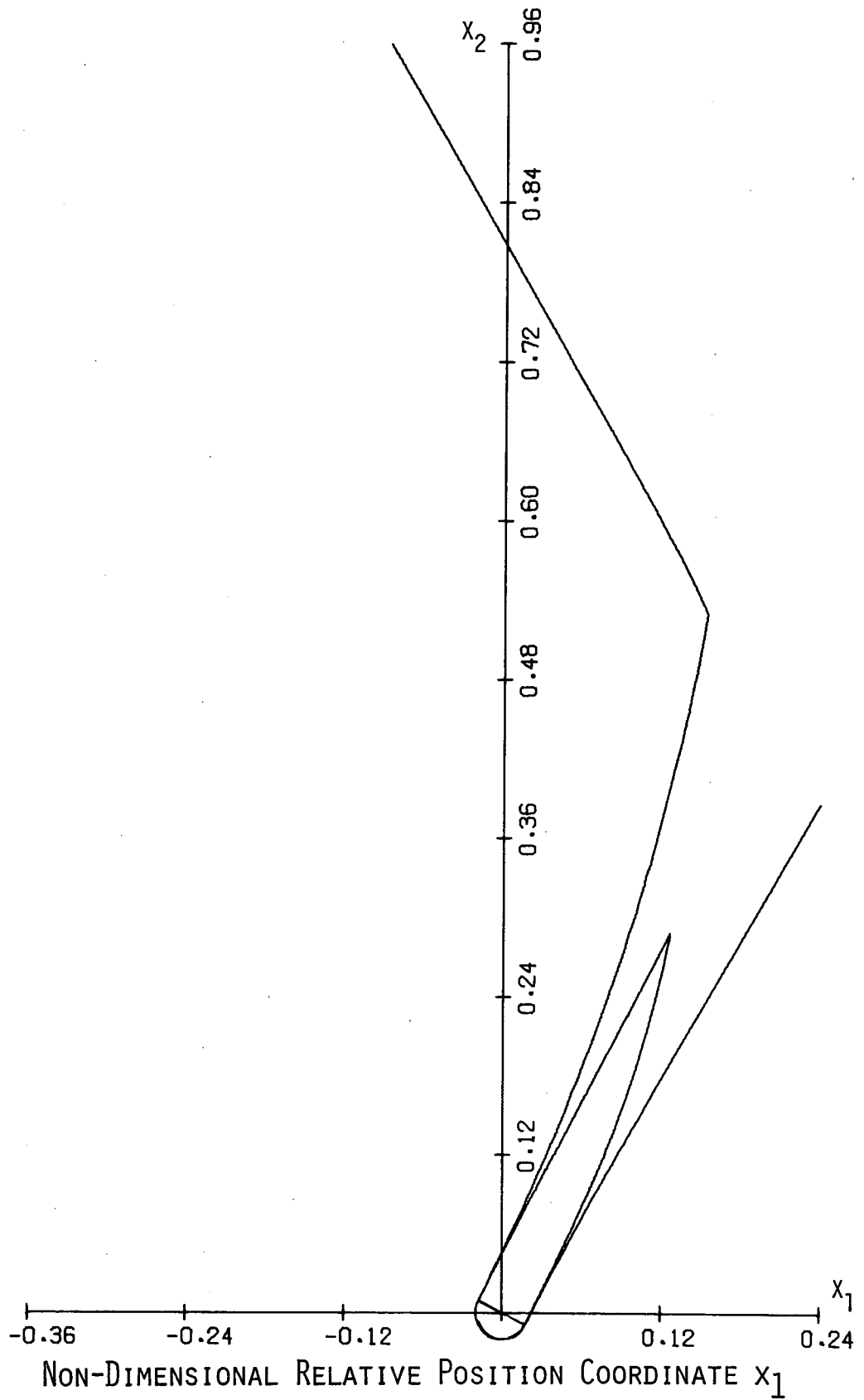


FIGURE 31 RED AND GREEN BARRIER CROSS SECTION AT $x_3=270^\circ$

occur. This same result occurs for points on the x_1 -axis arbitrarily close to the capture surface. The x_1 width of the green barrier at the x_1 -axis is then simply the diameter of the capture circle. On the other hand suppose the pursuer, still moving in the same direction as the (non-turning) evader, is well in front but only slightly to the left of the evader, say at $x_1 = 0.15$ and $x_2 = 0.75$ (yellow zone); from this position the pursuer can execute a hard right turn until a constant-line-of-sight collision course is obtained along which collision ultimately occurs. In fact the pursuer has enough time to execute such a maneuver from initial points further to the left of the evader with the limiting point being on the left green barrier. Thus the green barrier "expands" in front of the evader.

It is seen, from the $x_3 = 0^\circ$ cross-section, that the sides of the green barrier are straight lines except in the vicinity of the capture circle where they are portions of cycloids. From all initial points on the linear region of, say, the left green barrier, the pursuer makes a hard right turn until a constant-line-of-sight collision heading of $x_3 = 60^\circ$ is obtained. The resulting collisions all occur at the same point on the capture circle (see Figures 12 and 13). For initial points on the green barrier nearer the capture circle, however, the pursuer does not achieve a constant-line-of-sight collision heading and the resulting collisions occur at various points of the capture circle. In these cases the sides of the green barrier are curved near the capture circle.

These same expansion and curvature phenomena occur on the red barrier also, but the expansion differs somewhat by the fact that the evader is active on the red barriers. He is turning in an attempt to thwart the pursuer.

Examine now the $x_3 = 90^\circ$ cross-section (Figure 24). In this case, the pursuers velocity vector is initially directed parallel to the positive x_1 axis. If the pursuer is far to the right, the evader will be out of range by the time the pursuer performs a maneuver and no collision is possible. Thus the red and yellow zones are predominantly in the left half-plane where the danger of a collision is highest. The "corner" on the right green barrier is the point on the dispersal arc of Figure 11 at $x_3 = 90^\circ$. Below the corner the pursuer turns hard left; above he turns hard right. The $x_3 = 90^\circ$ cross-section is typical of all cross-sections from $x_3 = 0^\circ$ to $x_3 = 180^\circ$ with the exception that corners appear in the right green barrier only between $x_3 = 60^\circ$ and $x_3 = 120^\circ$ (Figure 11, the barrier intersections are asymptotic to $x_3 = 120^\circ$). There are also corners in the right red barrier but they occur only in the interval $x_3 \approx 52^\circ$ to $x_3 = 60^\circ$, corresponding to points on the dispersal curve "below" barrier intersections (Figure 5). In cases where red barrier corners do occur they are almost undetectable.

As previously mentioned, one of the major differences in the red and green barriers is that the right and left red barriers intersect. Consider the case where the pursuer is initially on the x_2 -axis far in front of the evader on a head-on ($x_3 = 180^\circ$) collision course (Figure 30). If the pursuer is sufficiently far in front of the evader,

the faster evader has ample time to turn and avoid a collision. Thus, beyond a certain distance, points on the x_2 -axis can not belong to the red zone; i.e., the right and left red barriers must intersect.

In examining the various cross-sections it is noted that the red zone is largest at the $x_3 = 180^\circ$ cross-section. For the Boeing 727 vs. Piper Commanche collision encounter, the $x_3 = 180^\circ$ red zone extends out to about 2,200 feet. In a head-on collision encounter this distance will be covered by the two aircraft in approximately three seconds! Thus the evader must never wait for the pursuer to approach the red zone before performing a collision avoidance maneuver, but must perform a maneuver while the pursuer is still in the yellow zone.

A Strategy for the Yellow Zone

Figures 32 to 38 show the green zones for $\alpha = 0.5$, $\delta = 2.5$, $R = 0.02$ superimposed on the red zones for $\alpha = 0.5$, $\delta = 2.5$ and various values of R . On each cross-section the locus of intersections of the right and left red barriers is a curve labeled Λ . If the initial state of the system is in the yellow zone to the left or right of Λ the evader should execute a hard right or left turn until the pursuer has at least moved into the green zone. If this strategy is continued sufficiently far into the green zone, the evader will maximize the minimum possible distance of closest approach.

NON-DIMENSIONAL RELATIVE POSITION COORDINATE x_2

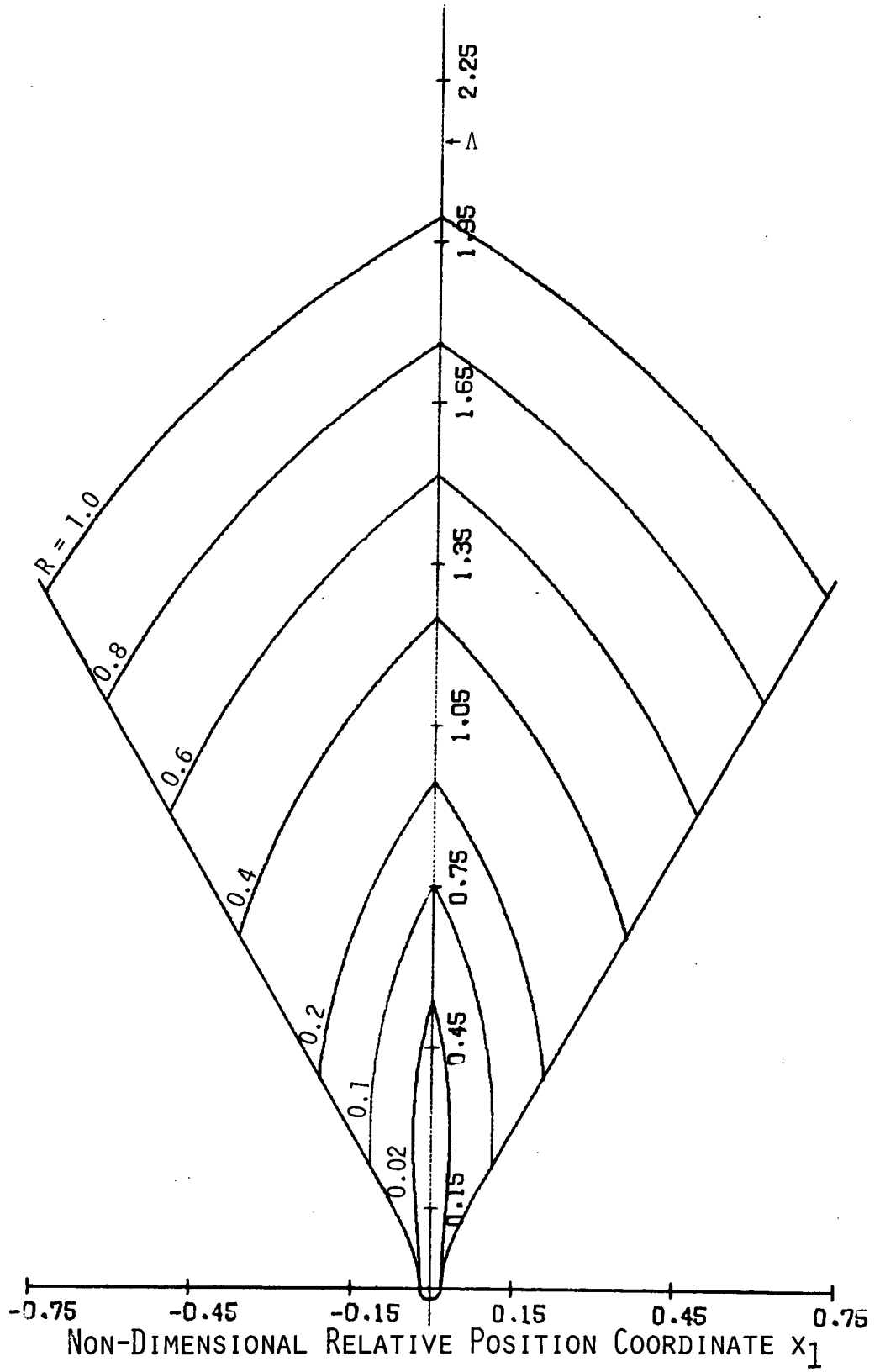


FIGURE 32 A STRATEGY FOR THE YELLOW ZONE $x_3=0^\circ$

NON-DIMENSIONAL RELATIVE POSITION COORDINATE x_2

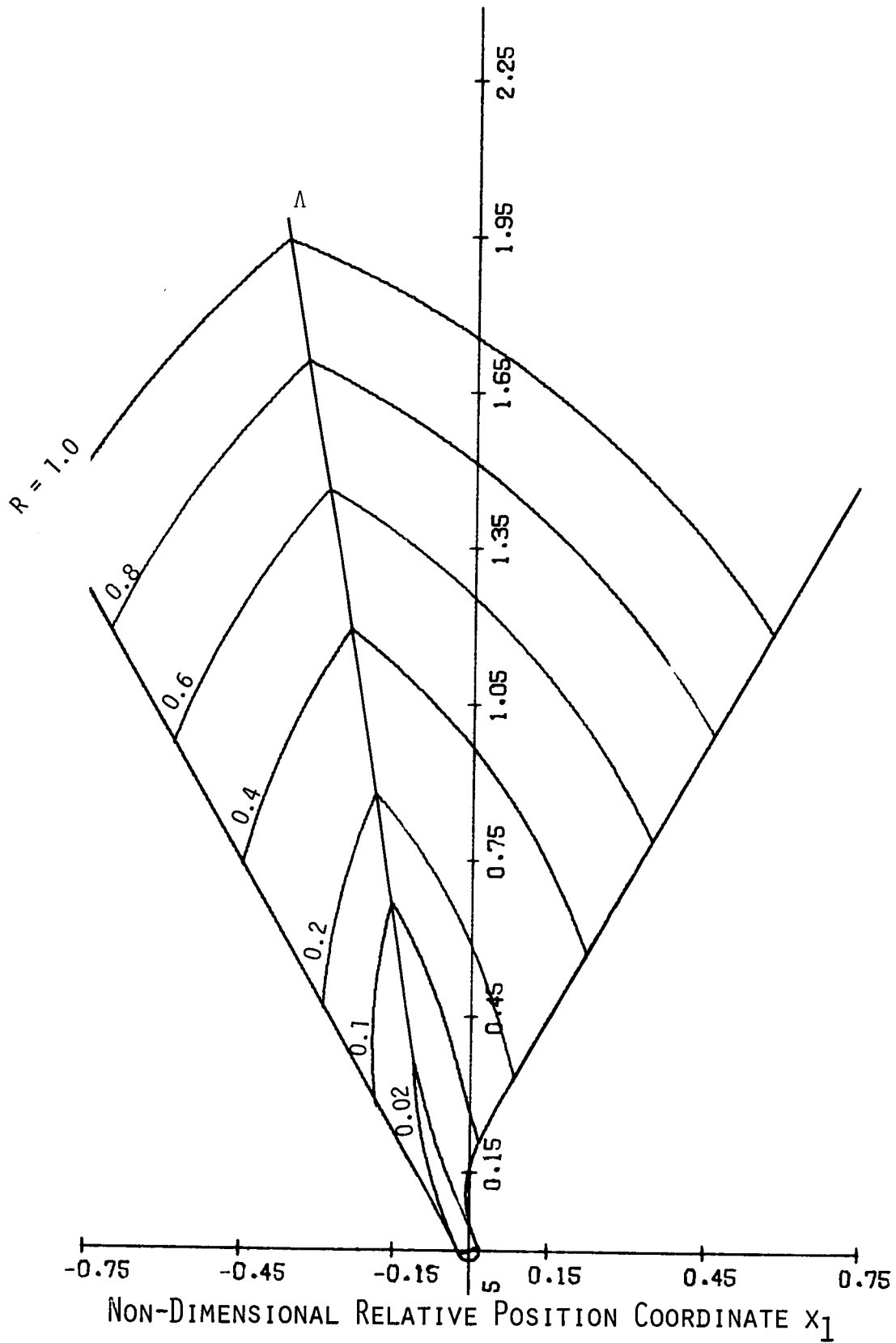


FIGURE 33 A STRATEGY FOR THE YELLOW ZONE $x_3=30^\circ$

NON-DIMENSIONAL RELATIVE POSITION COORDINATE x_2

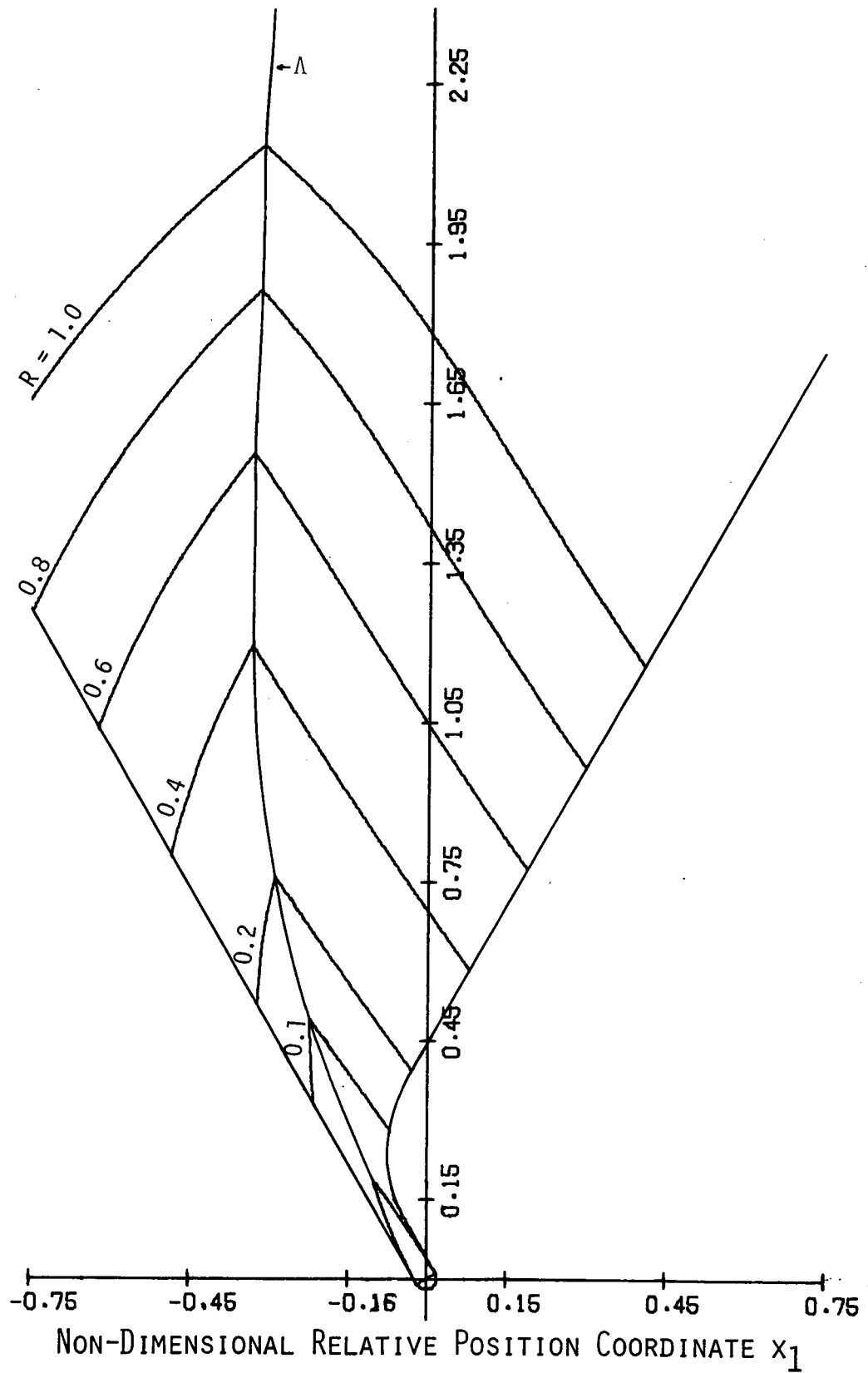


FIGURE 34 A STRATEGY FOR THE YELLOW ZONE $x_3=60^\circ$

NON-DIMENSIONAL RELATIVE POSITION COORDINATE x_2

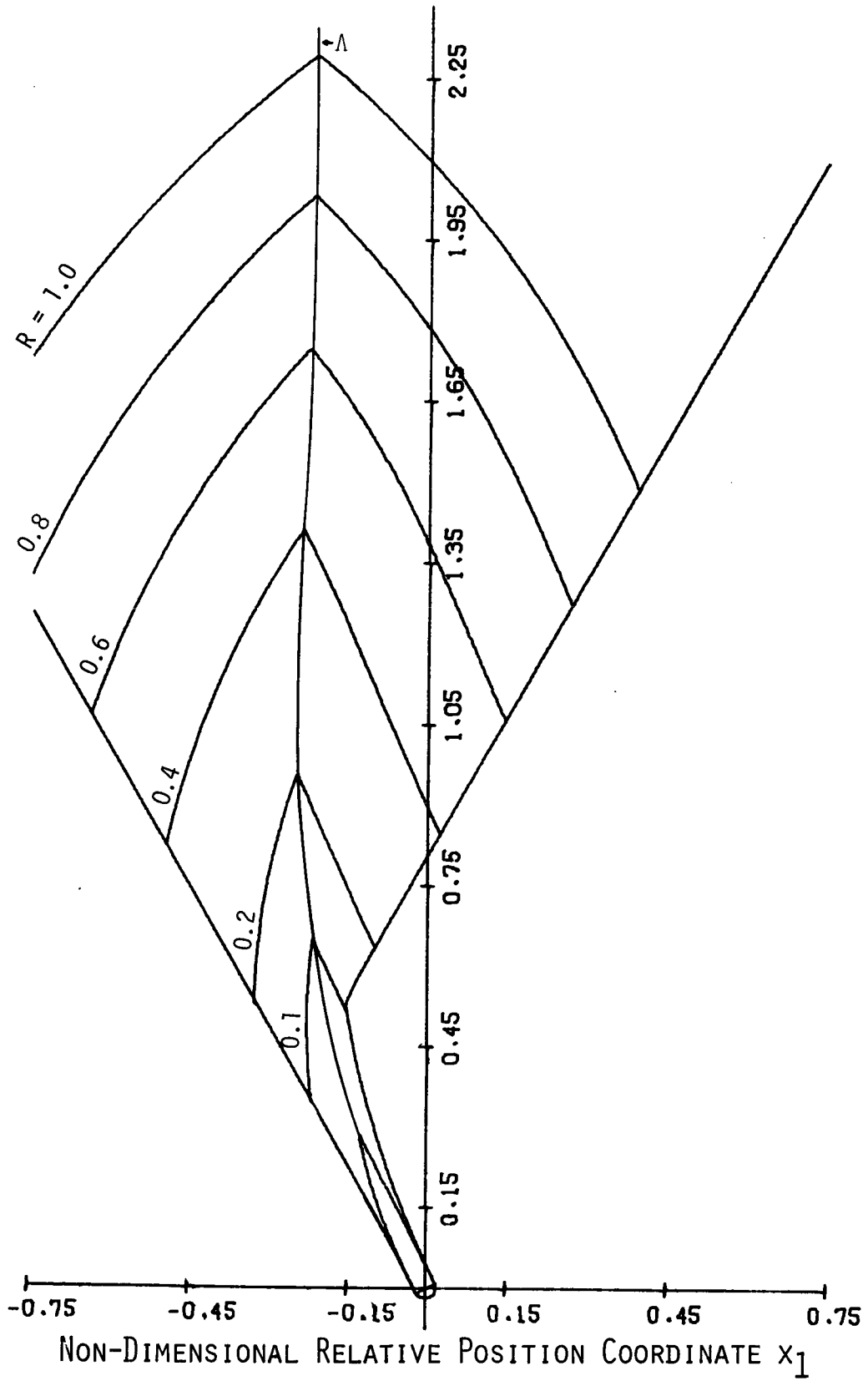


FIGURE 35 A STRATEGY FOR THE YELLOW ZONE $x_3=90^\circ$

NON-DIMENSIONAL RELATIVE POSITION COORDINATE x_2

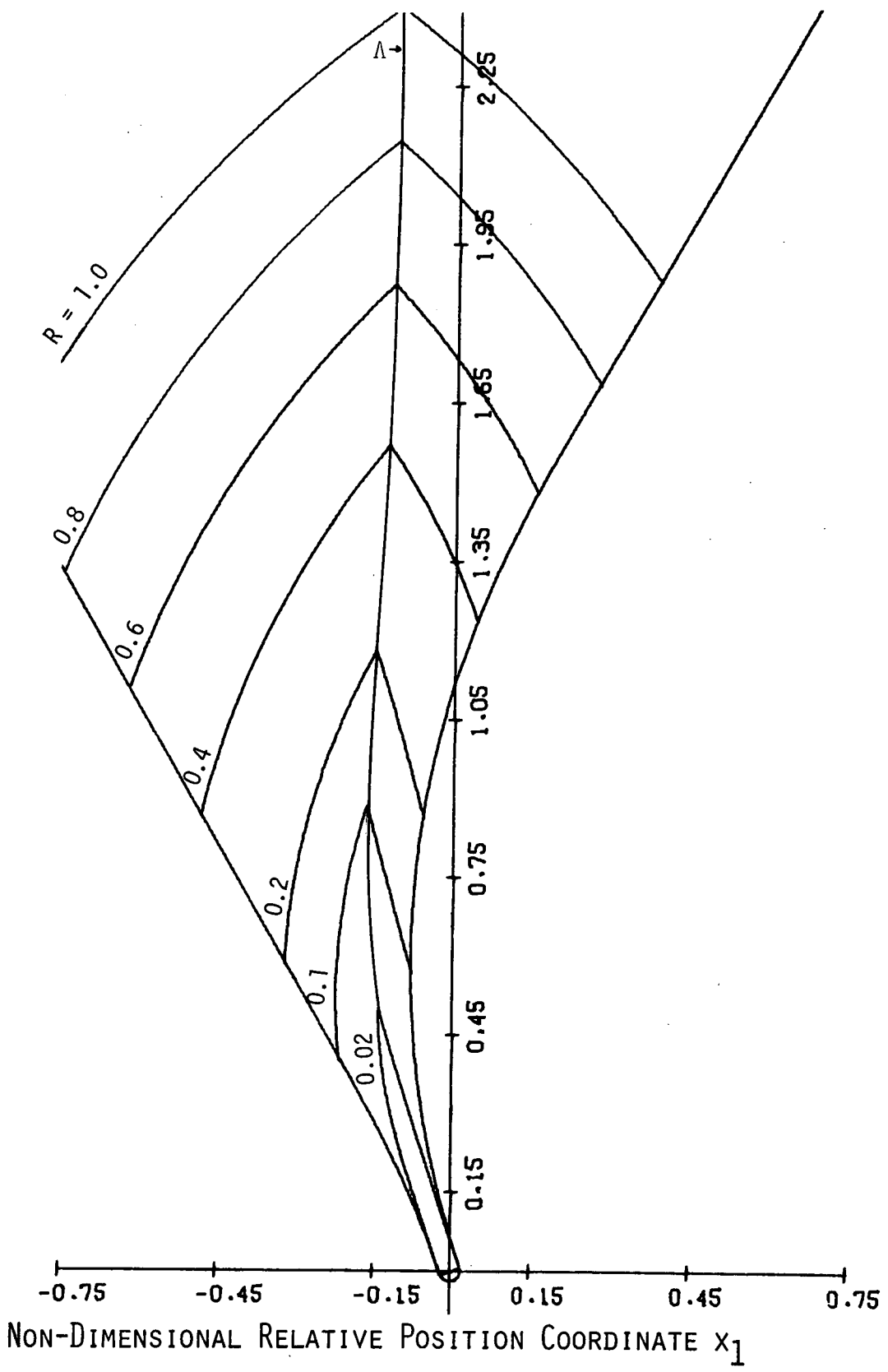


FIGURE 36 A STRATEGY FOR THE YELLOW ZONE $x_3 = 120^\circ$

NON-DIMENSIONAL RELATIVE POSITION COORDINATE x_2

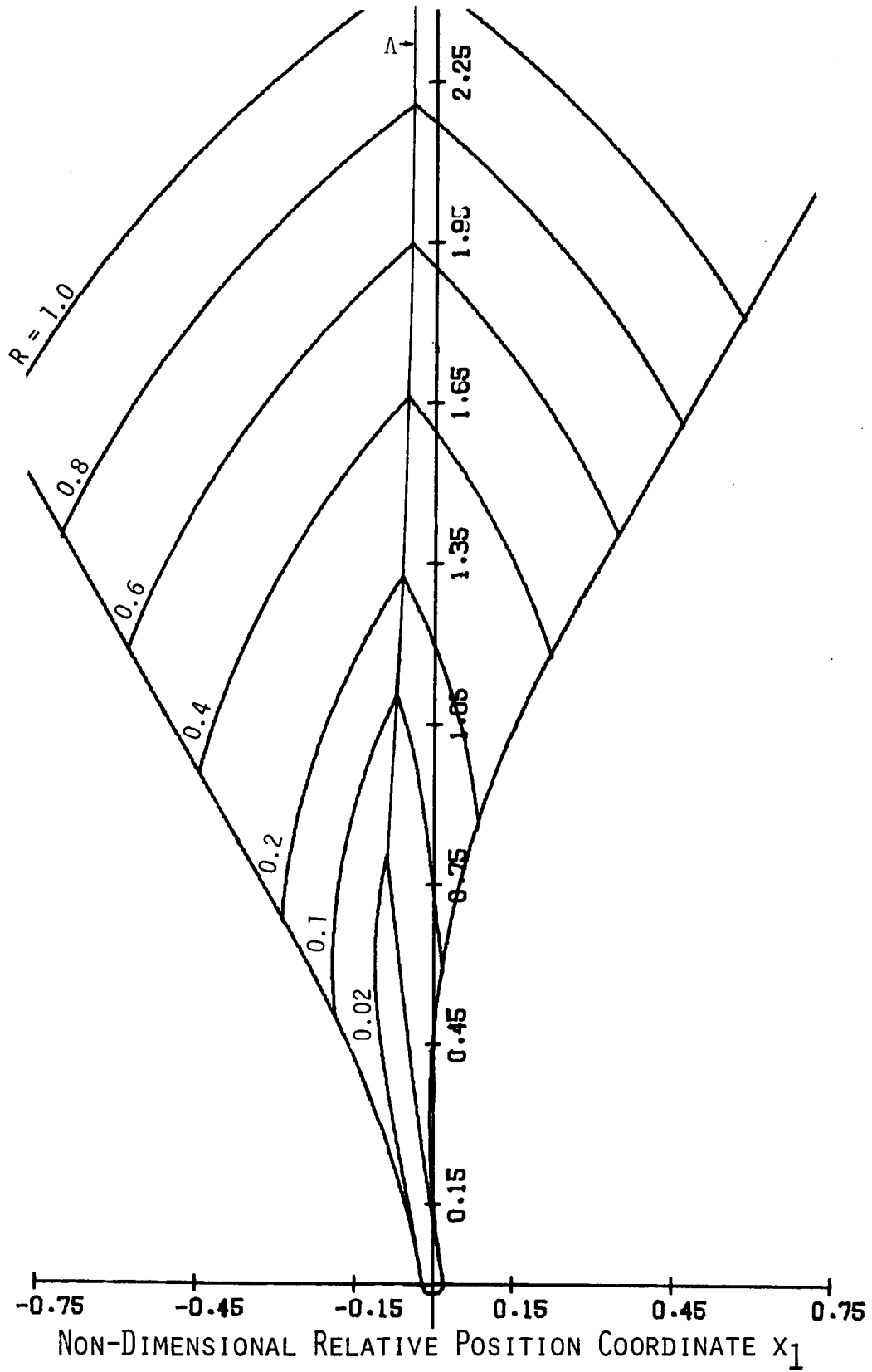


FIGURE 37 A STRATEGY FOR THE YELLOW ZONE $x_3=150^\circ$

NON-DIMENSIONAL RELATIVE POSITION COORDINATE x_2

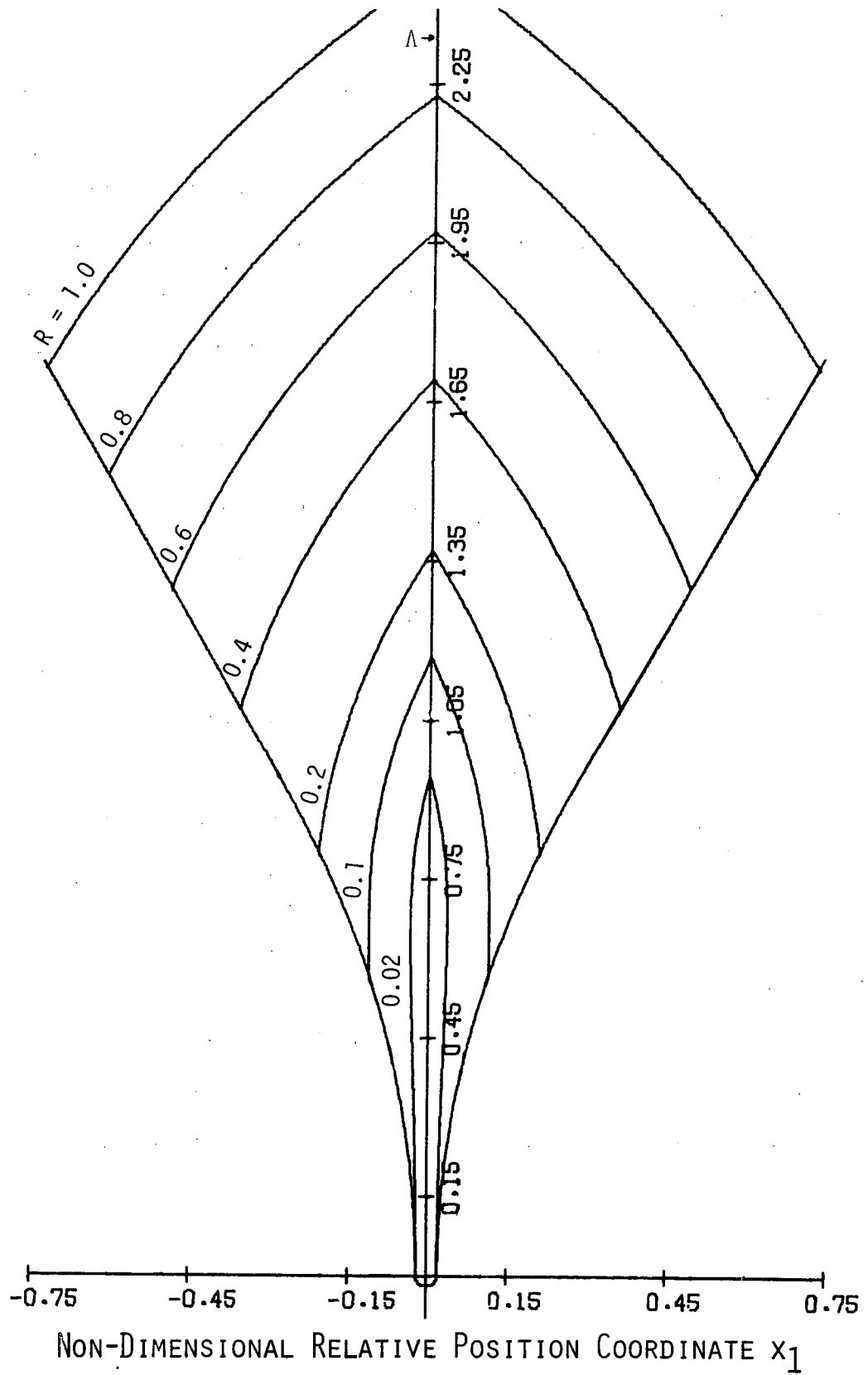


FIGURE 38 A STRATEGY FOR THE YELLOW ZONE $x_3=180^\circ$

Unknown Pursuer Heading

As previously mentioned, an entire collision avoidance maneuver can not be observed with respect to only one x_3 cross-section of the red and green barriers since x_3 changes during the maneuvers. Thus the use of the cross-sections presented so far in this report requires that the evader have knowledge of the pursuer's true heading. If this data is not available, but the turning rate ratio (δ) and the velocity ratio (α) are, then the evader may make use of Figure 39 in which the red zone with unknown pursuer heading is the union of all true red zones for $x_3 = 0^\circ$ to $x_3 = 360^\circ$. Thus, from points within the "red zone" of Figure 39 there exists at least one heading for the pursuer such that he can cause a collision regardless of any evasive maneuvers taken by the evader. The green zone of Figure 39 is the smallest of the true left and right green zones and is composed of the $x_3 = 60^\circ$ left green zone and the $x_3 = 300^\circ$ right green zone. From every point in the green zone (the green zone excludes the green barrier) of Figure 39 it is impossible for the pursuer to cause a collision with the non-turning evader; this green zone is "safe" regardless of the pursuer's heading. However since a near-miss is still possible from the green zone, a factor of safety can be built into the results by simply increasing the size of R to met whatever requirements are deemed necessary.

Ship Collision Avoidance

While the character of the results will remain the same for different values of α , δ , and R (provided $\alpha < 1$, $\delta > 1$) the size and

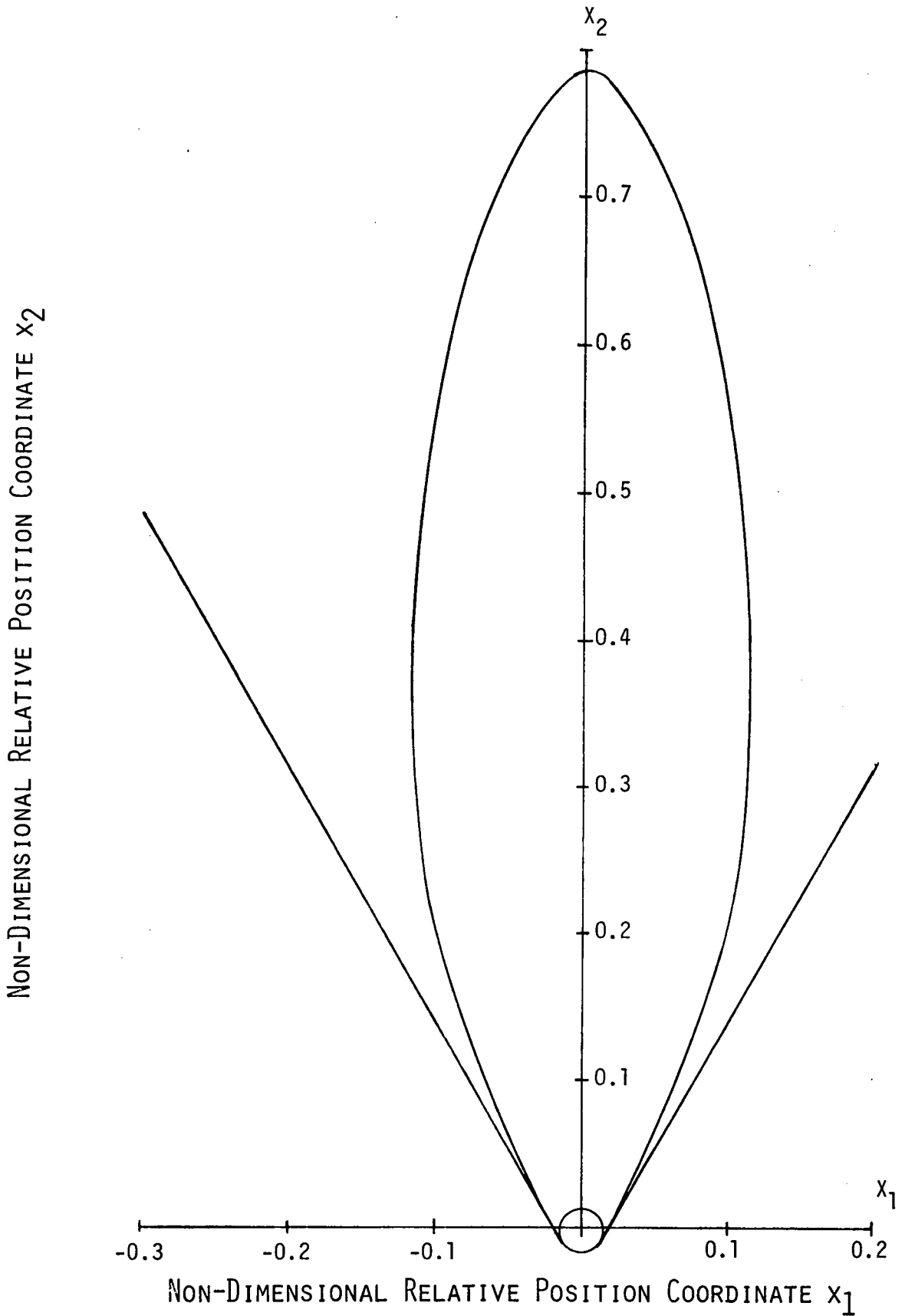


FIGURE 39 COLLISION AVOIDANCE ZONES FOR UNKNOWN PURSUER HEADING

shape of the red and green zones do vary somewhat dependent on the parameters used. To illustrate this point, parameters were chosen for a typical naval ship collision avoidance problem* ($\alpha = 0.8$, $\delta = 3.2$, $R = 0.1$) and the red and green barriers calculated. Results are shown in Figure 40 for the $x_3 = 180^\circ$ case. The "bulge" in the red zone is much more apparent in this case.

A Comparison of Results

Meier (Ref. 11, p. 514-521) obtained results for the "game of two cars" (Isaacs, Ref. 2) treating it as a game of degree. The "game of two cars" was formulated here as a game of kind and the solution used for the determination of the red barrier. The values for the parameters used here and by Meier are the same. Meier used a geometric construction to solve his problem, while an analytical approach was used here. The cross-sections obtained here agree with those published by Meier. However the strategies presented by him do not agree entirely with the strategies suggested here. Different strategies are not unexpected due to the fact that the strategies presented here are those for a game of kind rather than a game of degree. The strategies used here mini-max a Hamiltonian function with no performance index and keep the system on a barrier. Meiers strategies should mini-max a Hamiltonian function with a minimum time performance index and the system need not remain on the barrier.

*Evader - "Enterprise" Class Aircraft Carrier.
Pursuer - "Forrest Sherman" Class Destroyer.

NON-DIMENSIONAL RELATIVE POSITION COORDINATE x_2

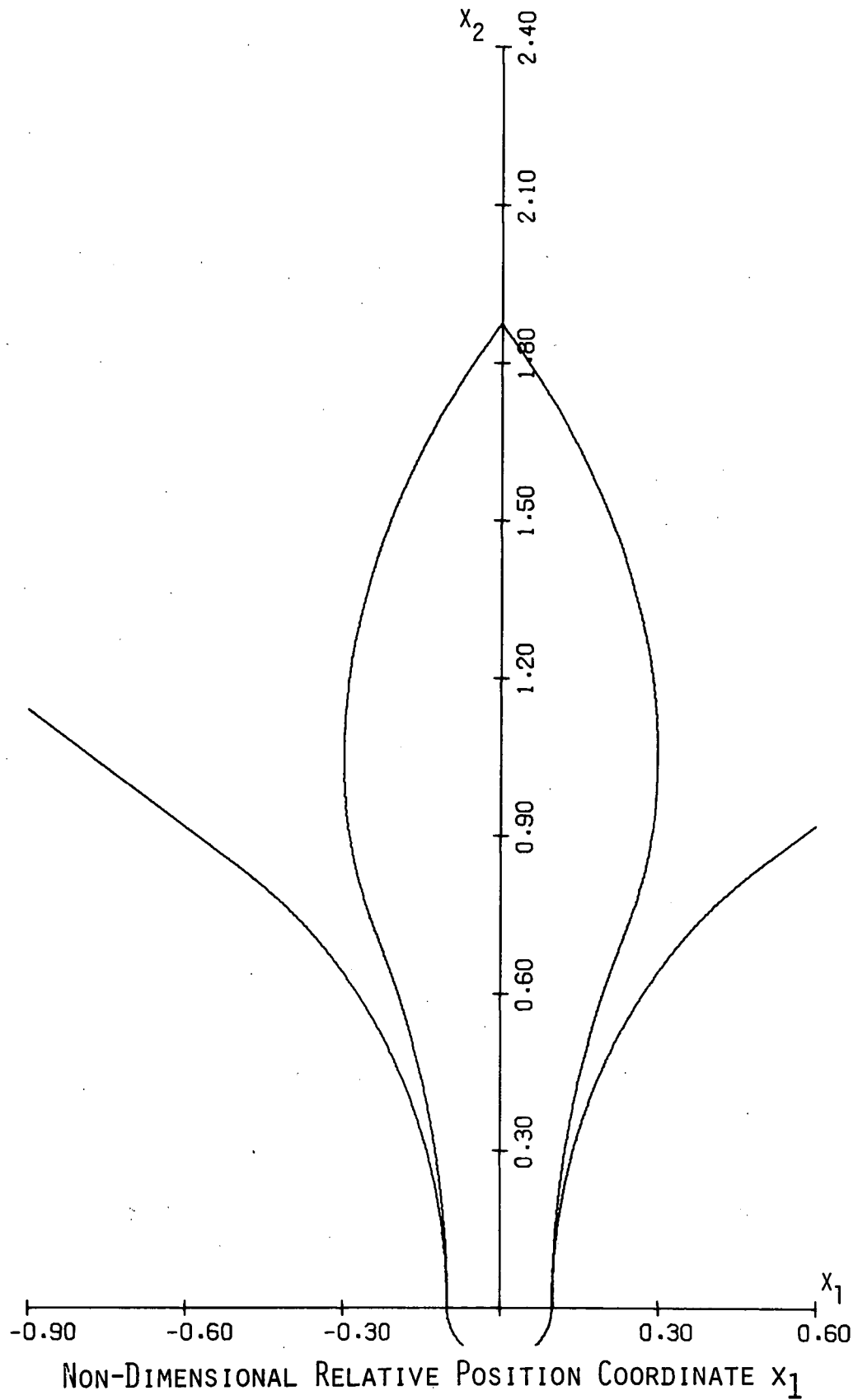


FIGURE 40 SHIP COLLISION AVOIDANCE

REFERENCES

1. Stodala, K. E., *"See and be Seen" Approached Analytically*, *Aeronautics and Astronautics, Letters*, Vol. 18, No. 10, October 1970.
2. Isaacs, Rufus, *Differential Games*, John Wiley and Sons, Inc., New York, 1965.
3. Grantham, W. J., *Controllability with State Constraints*, Ph.D. Dissertation, University of Arizona, 1973.
4. Lee, E. B., Markus, L., *Foundations of Optimal Control Theory*, Wiley, New York, 1967.
5. Balquiere, A., Leitmann, G., *On the Geometry of Optimal Processes*, *Topics in Optimization*, Edited by G. Leitmann, Academic Press, New York, 1967.
6. Blaquiere, A., Gerard, F., Leitmann, G., *Quantitative and Qualitative Games*, Academic Press, New York, 1969.
7. Kelley, H. J., Kopp, R. E., Moyer, G. H., *Singular Extremals*, *Topics in Optimization*, Edited by G. Leitmann, Academic Press, New York, 1967.
8. Halkin, H., *Mathematical Foundations of Systems Optimization*, *Topics in Optimization*, Edited by G. Leitmann, Academic Press, New York, 1967.
9. Grantham, W. J., Cliff, E. M., Vincent, T. L., *On Barriers in a Problem of Collision Avoidance*, *Proc. Fourth Int'l. Conf. on Systems Sciences*, University of Hawaii, January 1971.
10. Vincent, T. L., Goh, B. S., *Terminality, Normality, and Transversality Conditions*, *Journal of Optimization Theory and Applications*, Vol. 9, No. 1, January 1972.
11. Meier, L., *A New Technique for Solving Pursuit-Evasion Differential Games*, *Proceedings of the Joint Automatic Control Conference*, Boulder, Colorado, August 1969.